Kaunas University of Technology

Faculty of Mathematics and Natural Sciences

Investigation of the effect of the opening angle on the aerodynamics of a divergent jet

Master's Final Degree Project

Gauhar Kantayeva

Project author

Assoc. Prof. Dr., RUTKŪNIENĖ Živilė

Supervisor

Kaunas, 2020

Kaunas University of Technology

Faculty of Mathematics and Natural Sciences

Investigation of the effect of the opening angle on the aerodynamics of a divergent jet

Master's Final Degree Project

Applied Physics (6211CX015)

Gauhar Kantayeva

Project author

Assoc. Prof. Dr., RUTKŪNIENĖ Živilė

Supervisor

Dr. KNIZIKEVIČIUS Rimantas

Reviewer

Kaunas, 2020

Kaunas University of Technology

Faculty of Mathematics and Natural Sciences

Gauhar Kantayeva

Investigation of the effect of the opening angle on the aerodynamics of a divergent jet

Declaration of Academic Integrity

I confirm that the final project of mine, Gauhar Kantayeva, on the topic „Investigation of the effect of the opening angle on the aerodynamics of a divergent jet" is written completely by myself; all the provided data and research results are correct and have been obtained honestly. None of the parts of this thesis have been plagiarised from any printed, Internet-based or otherwise recorded sources. All direct and indirect quotations from external resources are indicated in the list of references. No monetary funds (unless required by Law) have been paid to anyone for any contribution to this project.

I fully and completely understand that any discovery of any manifestations/case/facts of dishonesty inevitably results in me incurring a penalty according to the procedure(s) effective at Kaunas University of Technology.

Gauhar Kantayeva
(name and surname filled in by hand)

(signature)

Kaunas University of Technology

Faculty of Mathematics and Natural Sciences

Topic of the project	Investigation of the effect of the opening angle on the aerodynamics of a divergent jet
Requirements and conditions (title can be clarified, if needed)	
Supervisor	Assoc. Prof. Dr., Živilė RUTKŪNIENĖ (position, name, surname, signature of the supervisor) (date)

Kantayeva, Gauhar. Investigation of the effect of the opening angle on the aerodynamics of a divergent jet. Master's Final Degree Project / Assoc. Prof. Dr., Živilė RUTKŪNIENĖ; Faculty of Mathematics and Natural Sciences, Kaunas University of Technology.

Study field and area (study field group): Physical sciences and Physics (C02).

Keywords: aerodynamics, a diverging jet, the opening angle, turbulent flow.

Kaunas, 2020. p.59.

Summary

Research object*:* aerodynamics of a diverging jet, the influence of the opening angle on the aerodynamics of a diverging jet.

Relevance: study of turbulent exchange in semi-limited jets and flows with the prospect of applying their results to clean the surface air basin.

Results*:* the thickness of the stream in a diverging conical and radial stream increases linearly with distance from the nozzle; an increase in the level of turbulence in diverging jets neutralizes a decrease in the width of the jet by increasing the cross section of the stream; at low frequencies of sound exposure, large vortices are first formed, then the intensity of the vortices decreases.

Conclusion: the change in the total thickness of the jet along its length occurs identically for a flat, cylindrical and conical diverging jet and obeys the dependence $\delta_{0.5} = 0.070x$.

Kantayeva, Gauhar. Atidarymo kampo įtakos difuzinės srovės aerodinamikai tyrimas. Magistro baigiamojo laipsnio projektas / Assoc. Prof. Dr., Živilė RUTKŪNIENĖ; Kauno technologijos universiteto Matematikos ir gamtos mokslų fakultetas.

Studijų kryptis ir sritis (studijų krypčių grupė): Fiziniai mokslai ir fizika (C02).

Reikšminiai žodžiai: aerodinamika, besisukanti srovė, atidarymo kampas, turbulentinis srautas.

Kaunas, 2020. p. 59.

Santrauka

Tyrimo objektas: besikeičiančios srovės aerodinamika, atidarymo kampo įtaka besikeičiančios srovės aerodinamikai.

Aktualumas: turbulentinių mainų pusiau ribotuose purkštukuose ir srautuose tyrimas, siekiant jų rezultatus pritaikyti valyti paviršiaus oro baseiną.

Rezultatai: besikeičiančioje kūginėje ir radialinėje srovėje srauto storis didėja tiesiškai, atsižvelgiant į atstumą nuo purkštuko; padidėjęs besisukančių purkštukų turbulencijos lygis neutralizuoja srovės pločio sumažėjimą, padidindamas srauto skerspjūvį; esant žemam garso poveikio dažniui, pirmiausia formuojasi dideli sūkuriai, tada sūkurių intensyvumas mažėja.

Išvada: bendro purkštuko storio pokytis išilgai jo ilgio vyksta vienodai, esant plokščiajai, cilindrinei ir kūginei besisukančiai srovei, ir priklauso nuo priklausomybės $\delta_{0.5}$ = 0.070x.

Table of contents

List of figures

List of tables

List of abbreviations and terms

Abbreviations:

x is the coordinate along the generatrix of the cone, m;

y - coordinate directed perpendicular to the generatrix of the cone, m;

R is the radius of the cone at the nozzle exit, m;

σ - the initial thickness of the jet, equal to the width of the output annular gap, m;

δ_m is the conditional thickness of the wall boundary layer, the distance from the wall to the point where $u = u_m$, m;

$\delta_{0.5}$ - conventional thickness of the jet, the distance along the normal from the surface and cone to the point where $u = 0{,}5 \cdot u_m$, m;

x_n - the length of the initial section of the jet, m;

S R - parameter of transverse curvature, $S_R = \frac{6}{R}$

u_0 is the initial velocity of the jet, m / s;

w - half angle at the top of the cone, grad;

τ_w - voltage friction in the boundary layer, kg / m· s;

δ^x - thickness of displacement, m;

δ^{xx} is the thickness of the pulse loss, m;

Re_0 is the Reynolds number according to the initial conditions of the jet, $Re_0 = \frac{u_0 6}{\nu}$;

F is the frequency of acoustic exposure, Hz;

S The number Strouhal number, $S = \frac{f \cdot 6}{u}$;

f_0 is the natural frequency of vortex formation, Hz;

c_p is the specific heat at constant pressure, J / kg K;

λ is the coefficient of thermal conductivity, m ^{2} / s;

ΔT - temperature difference on the surface of the cone and the environment, $\Delta T = T_w - T_0$, K;

A - is the local heat transfer coefficient of chi, W / m ^{2} K;

Pr - h The number Prandtl, $Pr = \nu / \alpha$;

Nu_x - is the Nusselt number, $Nu_x = \frac{\alpha \cdot x}{\lambda}$.

St - is the Stanton number, $St = \frac{q}{\rho c_p (T_w - T_0) u}$.

Indices

0 - initial condition at the nozzle edge;

0.5 - conditions in the outer layer, where $u = 0{,}5 u_m$;

m - conditions at the point of maximum speed $u = u_m$;

w - conditions on the wall ;

∞ —conditions at the outer boundary of the jet .

Introduction

Relevance and novelty of the topic. Recently, the study of turbulent exchange in semi-limited jets and flows has become more relevant, in connection with the prospect of using their results for cleaning the surface air basin. In the existing works, the laws of aerodynamics were considered for the longitudinal streamlining of a flat plate, cylinder, and ball, for which the basic laws of flow were revealed. One of the varieties of semi-bounded flows is the jet flow around a round cone, the study of which is devoted to few works. Based on these judgments, would the following goals be set for this work:

1 A detailed and systematic study of the fields and average pulsation velocity values in a turbulent semicircular nozzle that propagates over the surface of a cone and a disc at different values of the opening angle *w*, the transversal curvature parameter S_R and the divergent nozzle Reynolds *Re* number.

2 Qualitative and quantitative study of the influence of the aerodynamic geometry of the surface, direction of flow and acoustic effect on the vortex process in the initial part and development of turbulence in the transition sections and partially delimited rays that propagate along the smoothly flowing sample surface.

3 Based on the semi-empirical calculation and the analysis of experimental data, we obtain generalized dependencies related to the maximum speed and thickness of the boundary layer with longitudinal coordinates, taking into account the influence of the Reynolds number, such as cone, exit and cross direction. Curvature parameter suitable for the practical calculation of partially limited currents.

All this determined the objectives of the study, which boil down to the following:

1. To study the influence of the transverse curvature parameter, the cone angle, and the direction of the jet outflow on the dynamic characteristic in the initial, transitional, and main sections of the semi-limited jet.

2. Obtain detailed qualitative and quantitative data on the influence of the initial thickness of the jet, the opening angle and direction of the jet on the development of the boundary layer, the pulsation of the velocity, frequency and intensity of discrete vortices in sections.

3. To study the possibilities of controlling the development of turbulence using the directed influence of the acoustic field.

4. To study the influence of the transverse curvature parameter, the cone angle of the conical and radial jets in a wide range of variation of the curvature parameter $S_R = \sigma / R$, the Reynolds number and the cone angle.

1 Summary of works on aerodynamics of semi-limited and jet flows

1.1 General laws of semi- limited jets

The movement of jets of a viscous liquid or gas bounded on one side by a solid surface, both rectilinear and curved, is a form of flow that is very common in the art. The system of wall jet flows of different geometry with nonlinear generators most interesting is the problem of jet traveling along a cone with a vertex angle *w*, with the initial radius *R* of the nozzle on a section issuing from the annular gap width, σ. Moreover, the jet along the cone can propagate both from the top towards the base (diverging stream), and from the base towards the top (converging stream). Then some semi-bounded jet flows can be considered as a special case of a jet along a cone. In particular: for $w = 0, S_R \to 0$ $(R \to \infty)$, a plane semi-bounded jet is obtained, for $w = 0, S_R$ - finite, we have a jet along a cylindrical surface, for $w = \pi / 2$ *and* S_R - the finite jet along the cone passes into a radial stream propagating over the surface of the disk, for $w = 0$ and, $S_R \to \infty$, a free round stream is obtained (Figure 1). There are a large number of theoretical and experimental works devoted to the study of the laws of these semi-bounded jet flows. Since the objective of this work is to study the influence of the geometry of a streamlined surface on the aerodynamics and heat transfer of semi-limited jets, we consider only those works that are directly related to the subject under study.

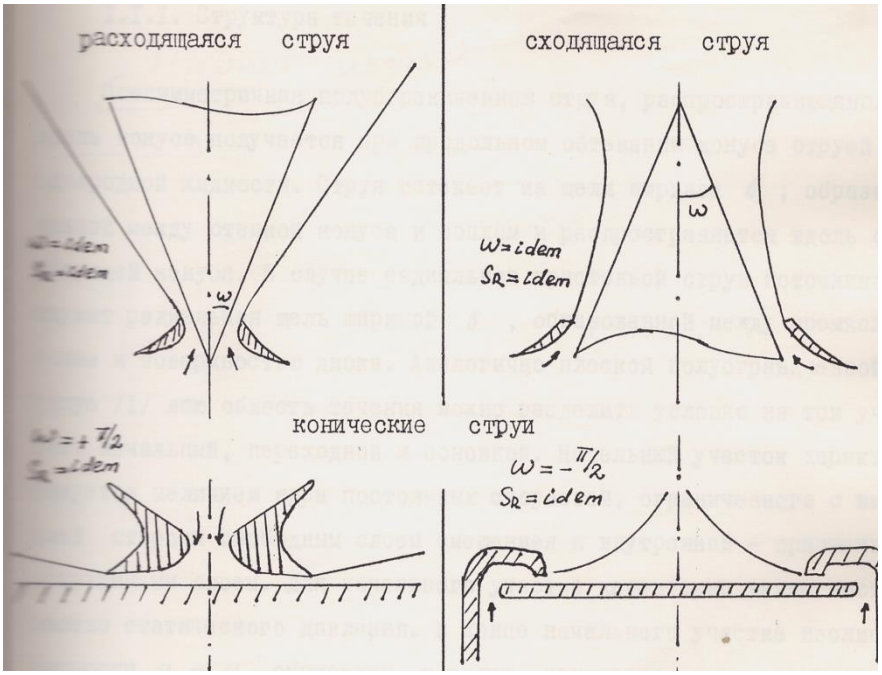

a)

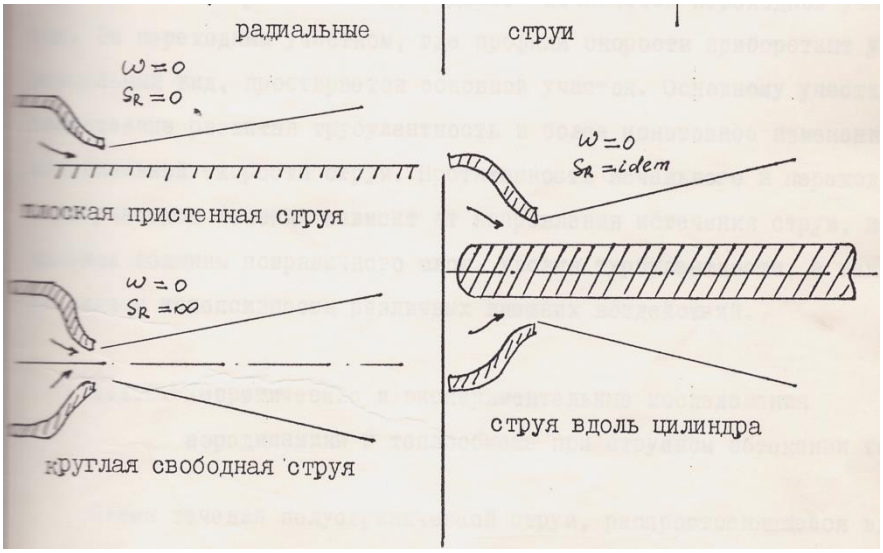

b)

Fig. 1. Diagram of jet flows of diverging and converging jets;
a) conical jets; b) radial jets: flat wall and round free jets, jet along the cylinder

1.1.1 The structure of the flow

The subject of the study, the jet propagating along the cone is obtained by longitudinal flow around the cone with a stream of a homogeneous liquid. With a true expiring from a slit wide, $\mathcal{O}$; formed between the wall of the cone and the nozzle and extends along the generatrix of the cone. In the case of a radial wall jet source is a radial gap of width, $\mathcal{O}$, formed between the nozzle edge and the disk surface. Similarly to a plane semi-bounded jet, the entire flow region can be conditionally divided into three sections: initial, transitional, and main. The initial section is characterized by the presence of a core of constant speeds, limited on the outside by a free mixing layer and the inner by a wall boundary layer. The initial section is also characterized by constant static pressure. At the end of the initial section, the velocity contours $u = u_0$ close, and then the transition section begins. Behind the transition section, where the velocity profiles become universal, the main section extends. The main area is characterized by developed turbulence and a more monotonous change in the maximum jet velocity. The length of the initial and transitional sections of the flow depends on the direction of flow of the jet, the initial thickness of the boundary layer, the level of turbulence, as well as on the type and intensity of various external influences.

The formation of the flow structure and velocity fields in the jet part of the stream and in the fan stream when interacting with the restricting surface is determined, ceteris paribus, by the ratio of two temperatures: the temperature of the gas flowing out of the nozzle T_0 and the temperature of the medium T_{md} into which the jet flows. The foregoing is a consequence of the fact that the kinematic coefficient of viscosity of gases substantially depends on temperature [1].

Physically, this can be manifested by a possible change in the motion regimes in the flow, by a change in the viscous friction forces and, as a consequence, by a change in the injecting ability of the jet after the gas flows out of the nozzle. Consider the flow along the body, for example a circular cylinder with a diameter d. Also consider the fluid created by individual molecules that move randomly. The average distance a molecule travels between collisions with neighboring molecules is defined as the mean free path value λ. If λ is a sequence of magnitude less than the measured body weight, the flow occurs as a continuous substance in the body. The

molecules fall on the surface of the body so often that the body cannot distinguish individual molecular collisions and the surface feels liquid as a continuous medium. This flow is called continuous flow. The other end is that λ is in the same order as the body scale. Here, gas molecules are so distant (according to d) that collisions with the body surface rarely occur and the body surface can clearly feel any molecular effect. This flow is called free molecular flow. In aircraft flights, shuttle-like vehicles find free molecular flow at the outer end of the atmosphere, where the air density is very low, λ varies according to the shuttle size. There are transient situations in which flux can show certain properties of the continuous and free flow of molecules. Unlike continuous flow, these flows are often called "low-density flows". By far, the vast majority of practical aerodynamic applications involve continuum flows. Low-density and free molecule flows are just a small part of the total spectrum of aerodynamics. The change in the aerodynamic characteristics of the jet part of the flow, in turn, determines the intensity of convective heat transfer at the interface between the fan flow and the solid surface.

A change in the temperature of the gas and gas flowing out of the nozzle in the fan stream is caused by various reasons. In the jet part of the stream, the formation of temperature fields in the cross section is mainly determined by the injection of environmental gas into the jet part of the stream, in the fan stream, mainly by the processes of heat transfer from the gas to the heated material [2].

1.1.2 Aerodynamics: classification and practical goals

The difference between solids, liquids and gases may be presented in simplified terms as follows. Put a solid object in a large, closed container. A solid object will not change; its shape and borders will remain the same. Now add the liquid inside the container. The liquid will change its shape to fit the shape of the container and will take the same boundaries as the container to the maximum depth of the liquid. Now inject gas into the container. The gas will completely fill the container, taking the same boundaries as the container.

The word fluid is used to mean liquid or gas. The technical difference between a solid and a liquid can be represented as follows. When a force is applied tangentially to the surface of a solid, it will experience finite deformation, and the tangential force per unit area — shear stress — will usually be proportional to the magnitude of the deformation. On the contrary, when a tangential shear stress is applied to the surface of the fluid, the fluid will experience an ever-increasing strain, and the shear stress will usually be proportional to the rate of change of the strain.

The most fundamental difference between solids, liquids and gases is at the atomic and molecular levels. In a solid, molecules are packed so close to each other that their nuclei and electrons form a rigid geometric structure, “glued” together by powerful intermolecular forces. In a liquid, the distance between the molecules is greater, and although the intermolecular forces are still strong, they allow the movement of the molecules enough for the liquid to become “fluid”. In a gas, the distance between the molecules is much greater (for air under standard conditions, the distance between the molecules is on average about 10 times the molecular diameter). Consequently, the influence of non-molecular forces is much weaker, and the movement of molecules occurs quite freely throughout the gas. This movement of molecules in gases and liquids leads to similar physical characteristics, the characteristics of a liquid are very different from those of a solid. Therefore, it makes sense to classify the study of the dynamics of both liquids and gases under one common heading, called fluid dynamics. On the other

hand, there are certain differences between the flow of liquids and the flow of gases. In addition, different types of gases (say, N_2, He etc.) have different properties. Therefore, fluid dynamics is divided into three areas as follows:

Hydrodynamics - the flow of fluids; gas dynamics - gas stream; and aerodynamics is the flow of air.

These areas are by no means mutually exclusive; there are many similarities and phenomena between them. In addition, the word "aerodynamics" has gained a popular use, which sometimes covers two other areas [3].

Aerodynamics is an applied science with many practical applications in technology. Regardless of how elegant an aerodynamic theory can be, or how mathematically complex a numerical solution can be, or how complicated an aerodynamic experiment can be, all such efforts are usually aimed at achieving one or more of the following practical goals:

1. Forecasting forces and moments, as well as heat transfer to bodies moving in a liquid (usually in air).

2. Determination of flows moving internally through ducts.

1.1.3 Theoretical and experimental studies of aerodynamics in jet flow around bodies

The flow pattern of a semi-limited jet propagating along a cone is shown in Figure 3. Since the flow along the plate, the cylinder, and the semi-bounded radial jet are special limiting cases of a more general one, the flow along the cone is a round straight cone with a semi-angle at the vertex *w* with a hydraulically smooth surface. Arrange an infinitely thin annular source on the cone surface in a section with the radius *R*. Let a jet propagate from the annular source along the generatrix of the cone toward the base (Fig. 2). The coordinate origin is located at the nozzle exit, the *x* axis is directed along the generatrix of the cone in the direction of the jet, and the *y* axis is perpendicular to the generatrix of the cone.

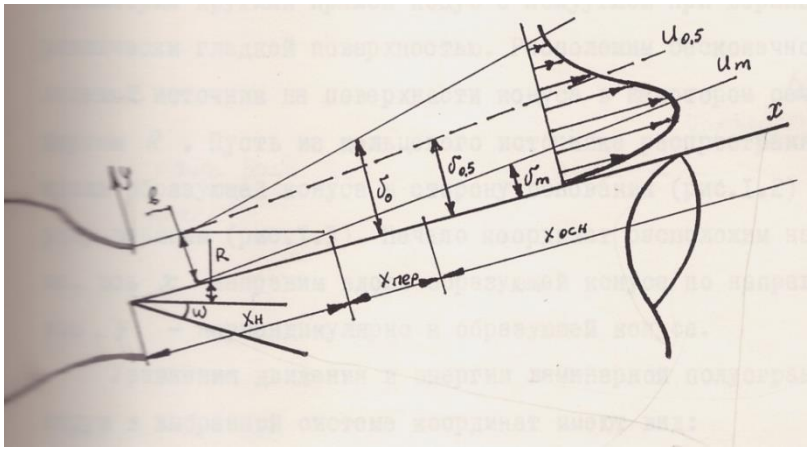

Fig. 2. Flow pattern of a conical diverging stream

The equations of motion (1) and energy of a laminar semi-limited jet (2) in the selected coordinate system have the form:

$$u\frac{\partial u}{\partial x} + v\frac{\partial u}{\partial y} = \nu\left(\frac{\partial^2 u}{\partial y^2} + \frac{1}{r}\frac{\partial u}{\partial y}\right) \quad (1)$$

$$u\frac{\partial T}{\partial x} + v\frac{\partial T}{\partial y} = \alpha\left(\frac{\partial^2 T}{\partial y^2} + \frac{1}{r}\frac{\partial T}{\partial y}\right). \quad (2)$$

And the continuity equation (3):

$$\frac{\partial(ru)}{\partial x}+\frac{\partial(rv)}{\partial y}=0. \quad (3)$$

Here r is the distance from the considered point of the jet to the axis of the jet, which is equal to formula (4):

$$r = R \pm x\sin w + y\cos w \quad (4)$$

Here, **"+"** refers to the case of a jet spreading from the top of the cone toward the base (diverging stream), **"-"** to the case of flowing from the base of the cone towards the top (converging stream). The boundary conditions are given as (5):

$u = v = 0$ for $y = 0$,

$u = 0$ for $y = \delta_0$,

$\frac{\partial u}{\partial y} = 0$ for $y = \delta_m$

$\Delta T = \Delta T_w$ for $y = 0$

$\Delta T = 0$, $\frac{\partial(\Delta T)}{\partial y} = 0$ for $y = \delta_0$ (5)

where $\Delta T = T\text{-}T_\infty$, T_w is the wall temperature, σ_m is the thickness of the written boundary layer, is equal to the distance from the wall to the point where $u = u_m$.

The problem of the propagation of a laminar jet along a flat surface was first solved by N.I. Akatnov. A feature of these works is that, using self-similarity transformations $u_m = Ax^{\alpha}$, $\varphi = B / Qx^{\beta}$, the system of partial differential equations describing the flow in a laminar wall jet is reduced to one ordinary differential equation that has an analytical solution.

The solution to the problem of the propagation of an annular laminar jet along a round cylinder is devoted to [4], in which it was suggested that the transverse curvature affects the dynamic parameters of the jet.

The system of the boundary layer equation (6) taking into account the swirl of the jet:

$$\begin{aligned}
&u\frac{\partial u}{\partial x}+\vartheta\frac{\partial u}{\partial y}-\frac{W^2}{x}=\frac{1}{\rho}\frac{\partial P}{\partial x}+\nu\frac{\partial^2 u}{\partial y^2};\\
&\frac{\rho W^2}{x}ctg\omega \;=\frac{\partial P}{\partial y};\\
&u\frac{\partial \omega}{\partial x}+\vartheta\frac{\partial \omega}{\partial y}+\frac{uW}{x}=\nu\frac{\partial^2 \omega}{\partial y^2};\\
&\frac{\partial(xu)}{\partial x}+\frac{\partial(x\vartheta)}{\partial y}=0;\\
&u\frac{\partial T}{\partial x}+\vartheta\frac{\partial T}{\partial y}=a\frac{\partial^2 T}{\partial y^2}.
\end{aligned} \quad (6)$$

Received for the case when:

$$x\sin\omega >> y\cos\omega. \quad (7)$$

Assuming the flow to be self-similar and constant, the momentum and momentum of the jet in any section of the cone, the following expressions (8) - (9) are obtained for the velocity components:

$$u = \frac{A}{x^{3/2}} \cdot F'(\varphi); \tag{8}$$

$$\vartheta = \frac{A}{4Bx^{5/4}} \cdot (5\varphi F' - 3F);$$

$$\omega = \frac{c}{x^{5/2}} \cdot F'(\varphi), \tag{9}$$

where $$\varphi = \frac{1}{2F_\infty}\left\{\ln\frac{F + \sqrt{F \cdot F_\infty} + F_\infty}{(\sqrt{F} - \sqrt{F_\infty})^2} + 2\sqrt{3}(arctg\frac{2\sqrt{F} + \sqrt{F_\infty}}{\sqrt{3F_\infty}} - arctg\frac{1}{\sqrt{3}})\right\},$$

$$F'(\varphi) = \frac{u}{u_m}, F_\infty = 1.7818;$$

A, B, C - to the constant.

The value of the Nusselt number for the average on the lateral surface of the cone has the form (10):

$$\overline{N}u = -4B\theta'_\sigma(\varphi)x^{-\frac{1}{4}}. \tag{10}$$

Obviously, by virtue of assumption (7), the results obtained (8-10) are applicable only for a jet close to radial.

The problem of the propagation of a laminar semi-limited jet along a cone both towards its base and towards the apex arising from an annular source of finite diameter was solved in detail by Isatayev I.S. [5].

Using the Stepanov and Mangler transforms (11):

$$\bar{x} = \frac{1}{L^2}\int_0^x r^2(x)dx, \bar{y} = \frac{r(x)}{L} \cdot y;$$

$$\bar{u} = u, \bar{\vartheta} = L\left[\frac{\vartheta}{r(x)} + \frac{1}{r^2(x)}\frac{dr(x)}{dx} \cdot u \cdot y\right]; \tag{11}$$

$$\bar{u} = u, \bar{\tau}_w = \frac{\tau_w}{r(x)};$$

$$\bar{\delta}^x = r(x)\delta^x, \bar{\delta}^{xx} = r(x)\delta^{xx}.$$

Non-planar boundary layer equations (12):

$$u\frac{\partial u}{\partial x} + \vartheta\frac{\partial u}{\partial y} = \nu\frac{\partial^2 u}{\partial y^2};$$

$$\frac{\partial(ru)}{\partial x} + \frac{\partial(r\vartheta)}{\partial y} = 0. \tag{12}$$

They are reduced to the equations of a flat boundary layer (13):

$$\bar{u}\frac{\partial \bar{u}}{\partial x} + \vartheta\frac{\partial \bar{u}}{\partial y} = \bar{U}\frac{\partial \bar{U}}{\partial x} + \nu\frac{\partial^2 u}{\partial y^2};$$

$$\frac{\partial \bar{u}}{\partial \bar{x}} + \frac{\partial \bar{\vartheta}}{\partial \bar{y}} = 0. \tag{13}$$

The boundary conditions for both flows have the form (14):

$$u = \vartheta = 0 \qquad npu \qquad y = 0$$
$$u = U(x) \qquad npu \qquad y = \delta \tag{14}$$

where $U(x)$ - Ext speed e of the flow, it is zero for a semi-infinite jet.

Using expression (4), the Stepanov - Mangler transform can be reduced to the following form (15):

$$\bar{x} = \frac{1}{3L^2} \cdot (3R^2 x \pm 3Rx^2 \sin\omega + x^3 \sin^2\omega);$$
$$\bar{y} = \frac{1}{L} \cdot (R \pm x \sin\omega) \cdot y;$$
$$\bar{u} = u \tag{15}$$
$$\bar{\vartheta} = \left[\frac{\vartheta}{R \pm x \sin\omega} + \frac{y \sin\omega}{(R \pm x \sin\omega)^2} \cdot u \right] \cdot L;$$
$$\tau_w = \frac{1}{L} \cdot (R \pm x \sin\omega)\bar{\tau}_w.$$

Here L is the characteristic linear dimension. If we set the gap width σ, the nozzle radius R, and the jet outflow velocity u_0, then the integral invariant for a non-planar flow can be written in the form of formula (16):

$$E = \int_0^\infty ru\left(\int_y^\infty ru^2 dy\right)dy = \frac{1}{2} R^2 u_0^3 \sigma^2. \tag{16}$$

Moreover, the integral invariant for a plane flow has the form (17):

$$E = \frac{1}{2}\sigma^2 u_0^3. \tag{17}$$

Then the solution to the problem of the propagation of a semi-limited laminar jet flowing out of an annular gap of radius R along a conical surface is presented as follows (18):

$$u = \left[\frac{15E}{2\nu(3R^2 x \pm 3Rx^2 \sin\omega + x^3 \sin^2\omega)} \right]^{\frac{1}{2}} \cdot f'(\eta), \tag{18}$$

$f' = u / u_m$ is the velocity distribution function, which is related to the parameter $\bar{\eta}$ as follows , which is shown in formula (19) - (20):

$$\bar{\eta} = \ln \frac{\sqrt{1+\sqrt{f}+f}}{1-\sqrt{f}} + \sqrt{3} arctg \frac{\sqrt{3f}}{2+\sqrt{f}};$$
$$\eta = \left[\frac{E \cdot 135(R \pm x\sin\omega)^4}{32\nu^3(3R^2 x \pm 3Rx^2 \sin\omega + x^3 \sin^2\omega)^3} \right] \cdot y; \tag{19}$$

$$\vartheta = \left(\frac{135E\nu}{32}\right)^{\frac{1}{4}} \frac{(R \pm x\sin\omega)}{(3R^2 x \pm 3Rx^2 \sin\omega + x^3 \sin^2\omega)^{\frac{3}{4}}} (3\eta f' - f) \pm$$
$$\pm \left(\frac{40E\nu}{3}\right)^{\frac{1}{4}} \frac{(3R^2 x \pm 3Rx^2 \sin\omega + x^3 \sin^2\omega)^{\frac{1}{4}} \cdot \sin\omega}{(R \pm x\sin\omega)^2} \cdot \eta f'. \tag{20}$$

The friction stress on the wall has the expression in the form (21):

$$\tau_w = \rho\left(\frac{125E^2}{216\nu}\right)^{\frac{1}{4}} \frac{R \pm x\sin\omega}{(3R^2x \pm 3Rx^2\sin\omega + x^3\sin^2\omega)^{5/4}}, \quad (21)$$

The second volumetric flow rate of the liquid through the cross section of the jet is determined by the formula (22):

$$Q = 2\pi\left(\frac{40E\nu}{3}\right)^{\frac{1}{4}} \cdot \left(3R^2x \pm 3Rx^2\sin\omega + x^3\sin^2\omega\right)^{\frac{1}{4}} \quad (22)$$

The flow of the kinematic pulse through the cross section of the jet has the form:

$$K = 2\pi\left(\frac{750E^3}{\nu}\right)^{\frac{1}{4}} \cdot \frac{0.2223}{(3R^2x \pm 3Rx^2\sin\omega + x^3\sin^2\omega)^{1/4}} \quad (23)$$

For *w = 0, we* obtain the solution of a laminar semi-limited jet propagating along a cylinder with a radius *R*, found in [4] in the absence of a swirl.

At *w = 90* ° from equality (18-23), one can find a solution to the problem of the propagation of a radial semi-bounded jet flowing from a ring source with a radius R along a flat surface, obtained in [6].

In [6], the results obtained are generalized to the case of motion of a compressible gas. The equation of a compressible gas is transformed using the Dorodnitsyn variables and is solved under various boundary conditions for temperature. The influence of the Prandtl number, momentum, and other parameters on the velocity and temperature fields is determined, and the latter are compared with the corresponding fields in an incompressible fluid.

It was assumed that the turbulent friction on the wall is specified according to the Blasius law, and the turbulent friction in the external jet region is determined by the Prandtl formula. Later, using the same method in [7], a formula was obtained for calculating the friction coefficient c_f.

A theoretical solution of the problem of the motion of wall jet as in the above studies [2, 7], as in other similar operation [8] are found separately for the inside (the wall) and the outer part of the flow. Then, “stitching” of the obtained solutions is carried out along the line of maximum speed. The solution obtained in such a cumbersome way is not always convenient for practical use. In this case, the solution is constructed on the basis of analogy for the near-wall part of the jet with a flow in the channel, and for the external part, with a free stream. Since these analogies are not strict, the selected velocity profiles do not agree very well with the experimental ones.

By applying the unified velocity profile borrowed from the experiment in the entire cross section of the jet in the form of formula (24):

$$\frac{u}{u_m} = 1.426\eta^{\frac{1}{8}} \cdot (1 - 0.503\eta)^{\frac{3}{2}}, \quad (24)$$

where $\eta = y / \delta_{0.5}$

In [9], the same problem is solved by the method of integral relations. Having adopted the value of the friction resistance on the wall, we obtain the formula (25):

$$c_f = \frac{0.0225}{\mathrm{Re}_x^{0.10}}, \quad (25)$$

the author obtained expressions for calculating the change in the boundary and the maximum jet velocity in the form of formula (26):

$$\delta_{0.5} = 0.0609 \cdot (x + x_0);$$
$$u_m = \frac{4.80 \cdot A}{(x + x_0)^{0.561}}; \quad (26)$$

A and x_0 are quantities determined by the experimental conditions.

Among modern works that investigated a plane semi-bounded jet, we single out the papers [10-13]. A detailed analysis of both theoretical and experimental works on near- wall jet flows is given in [10]. The authors of [11] investigated in detail the laws of a planar semi-bounded jet for various values of the satellite parameter. The formulas he obtained for calculating the change in the maximum velocity and thickness of the jet for the case of a flooded jet *(m = 0)* have the form of formula (27):

$$\frac{u_m}{u_0} = \frac{4.29}{\left(x/\sigma + x_0/\sigma\right)^{0.534}};$$
$$\frac{\delta_{0.5}}{\sigma} = 0.0942\left(\frac{x + x_0}{\sigma}\right)^{0.954}. \quad (27)$$

1.2 The influence of the geometry of the streamlined surface and the acoustic impact on turbulence in the initial and transitional sections of free and semi-limited jets

At sufficiently large Reynolds numbers, all jet flows undergo qualitative changes during their motion — the transition of the laminar form to turbulent [14]. Experimental confirmation of the existence of such a transition in semi- limited jets with puddles of work [11, 13, 15, 16, 17] and others.

The theoretical study of the turbulence and hydrodynamic stability of various systems has been the subject of many works by both domestic and foreign authors [18–23] and others. The stability of time-periodic flows is considered in [21]. A general review of the problem of transition to turbulence is given in the monograph [22].

In real flows, various external influences have a significant effect on the transition from a laminar flow to a turbulent one.

The regularities of the laminar - turbulent transition of a semi-limited jet propagating over the surface of a flat plate were studied in [7, 17, 32]. The results of [11] and [24] show that a negative longitudinal pressure gradient causes a prolongation of the length of the laminar wall flow. An increase in the acceleration parameter and the longitudinal pressure gradient causes a significant decrease in the level of turbulence in the main section of the jet with distance from the nozzle.

The influence of the transverse curvature parameter and the Reynolds number on the laminar-turbulent transition and the development of turbulence in an annular jet propagating over the cylinder surface were studied by the author of [25]. They are found in the initial section of the jet presence of large vortices and have established the dependence of the frequency of formation of vortices on the Reynolds number and the parameter S_R. The existence of regular vortex structures in free jets was noted by the secrets of earlier works [26–29]. By external periodic action, the aerodynamic and thermal characteristics of the jet can be significantly changed [29–34].

In the experiments of Isatayev S.I. et al. [11, 35] investigated the effect of acoustic impact on the aerodynamics of a wall jet and the burning rate of a propane - air jet torch. It was found that resonant acoustic exposure significantly intensifies the combustion of propane - air mixture, because large-scale vortices arising from acoustic exposure significantly enhance the mixing of fuel with oxygen in the environment. The resonant effect on the semi-limited jet leads to a decrease in the length of the wall laminar boundary layer and the region of developed turbulent flow approaches the mouth of the nozzle. Exposure to high-frequency oscillations delays the laminar - turbulent transition.

The pulsation structure of a radial semi-bounded jet was studied in [36], in which the authors showed that the distribution of the velocity pulsations is independent of the parameter S_R and the Reynolds number, and also found a wall maximum of the pulsations of the velocity upon injection. A formula is given that determines the beginning of the self-similarity region for pulsation velocities for various values of the parameters of injection and suction.

1.3 Research objectives

Those who have worked on the flow around a flat plate, a cylinder and a diverging cone are disconnected and need to find a regularity for all.

All this determined the objectives of the study, which boil down to the following::

To study the influence of the transverse curvature parameter, the cone angle, and the direction of the jet outflow on the dynamic characteristic in the initial, transitional, and main sections of the semi-limited jet propagating along the conical and radial surfaces in a wide range of variation of these parameters and the initial Reynolds number.

Obtain detailed qualitative and quantitative data on the influence of the initial thickness of the jet, the opening angle and direction of the jet on the development of the boundary layer, the pulsation of the velocity, frequency and intensity of discrete vortices in the initial, transitional and main sections of the diverging jet.

To study the possibilities of controlling the development of turbulence using the directed influence of the acoustic field.

To study the influence of the transverse curvature parameter, the cone angle of the conical and radial jets in a wide range of variation of the curvature parameter $S_R = \sigma/R$, the Reynolds number and the cone angle.

On the basis of experimental data, obtain generalizing semi-empirical formulas for calculating aerodynamic characteristics that take into account the influence of the transverse curvature parameter, the opening angle and the direction of the jet flow, suitable for practical use.

2 Experimental installations and measurement technique

The experimental setup was a jet type wind tunnel, the main components of which were fabricated according to the method described in [37–40]. The installation met all the requirements of a modern aerodynamic experiment and had the following advantages:

1 The ability to smoothly vary the speed of the jet at the exit of the nozzle in the range from 5 to 80 m / s.

2 Vibration resistance .

3 Low level of turbulence and close to a rectangular velocity profile at the nozzle exit.

4 High degree of alignment of the nozzle and the working fluid.

5 Changeable parameter S_R .

6 Before the experiments, the constancy of the following quantities was carefully controlled:

7 The width of the gap between the nozzle and the surface of the working fluid at the outlet section.

8 Symmetry of the jet.

9 The value of speed and its profile at the exit of the nozzle.

10 Ambient and jet temperatures.

11 Local atmospheric pressure.

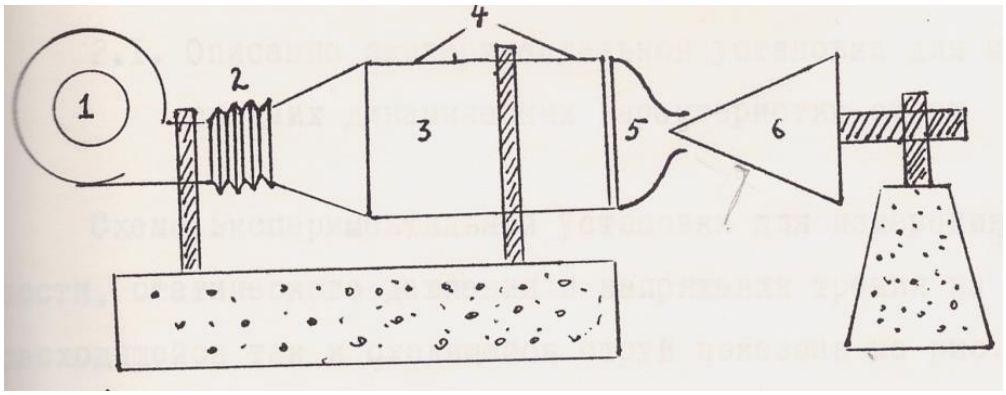

1 - fan, 2 - rubber joint,
3 - stilling chamber, 4 - leveling nets,
1 - profiled nozzle, 6 - working fluid, cone or disc.

Fig. 3. Scheme of the experimental setup:
diverging stream

2.1 Description of the experimental setup for studying the average dynamic characteristics of the jet

The experimental setup for measuring the average velocity, static pressure, and friction stress on the wall of a diverging jet is shown in Figure 3. Air was supplied by fan 1, through a rubber joint 2 and a diffuser, into a stilling chamber 3, with leveling grids 4, and flowing out of a nozzle 5 along a cone or disk 6 into a stationary air environment. The profiled nozzle according to the Vitoshin formula provided a smooth speed profile at its outlet. In order to avoid undesirable turbulence in the first part of the nozzle, all the internal elements of the device had an aerodynamic shape. The fan was a TV-80-1.6 centrifugal fan. The compression ratio of

nozzles made of plexiglass, duralumin and steel is 20 to 45. A circular disc with a carefully polished surface was used as the working medium, the purity of which corresponds to the hydraulic smoothness and the duralumin cones. The cone angles were 15°; 30°. The length of the measuring section extended to 500 mm. The parameter S_R was regulated by the longitudinal movement of the cone along the axis of the nozzle, as well as the use of nozzles of various diameters.

The sensors were moved using a coordinator along the surface of the cone with an accuracy of 0.1 mm, perpendicular to the surface with an accuracy of 0.01 mm. The initial reference position of the full pressure tube was determined by breaking its electrical contact with the metal surface of the working fluid.

2.2 An experimental setup for studying the pulsation characteristics and the vortex structure of the flow

The layout of the experimental setup for studying turbulent jet processes is shown in Figure 4. In this work, we used a system of hot - wire anemometric equipment developed in the research laboratory of heat transfer and combustion of KazNU named after Al-Farabi.

For visual examination, the working section of the installation was placed in the field of view of the IAB-451 shadow device (9, fig .4). A complex of equipment was placed nearby to study the processes of natural vortex formation and acoustic impact on the jet. A loudspeaker 7 with a power of 25 W with a protective casing 8 was installed in the lower part of the still chamber and, if necessary, created a sound wave field directed vertically upstream of the stream. The cover on the outside was covered with plastic wrap to improve the performance of the speaker. The inner wall of the chamber is coated with sound-absorbing material necessary to prevent unwanted resonance.

To visualize the air stream, the air flow was heated in a still chamber to a temperature of 35° - 40° using a grid 26, through which a current was passed from an autotransformer. To visualize the boundary layer near the wall of the cone and the boundary of the jet, additional elements are provided for heating the cone and nozzle. For further processing, the picture of vortex structures was photographed with a Zenit-type reflex camera.

The basis of the measured medium and pulsation amounted speed laid known principle of automatic maintenance of the temperature sensor included in the arm of the bridge termoanemometr DC (Figure 5). If the sensor thread is heated in the absence of flow to a certain temperature, the bridge is balanced, then the thread is introduced into the flow, then the thread gives off a certain amount of heat and its resistance changes. The resulting voltage imbalance of the bridge is amplified by a feedback amplifier (SLA). Signal unbalance is fed to the power amplifier (PA), then the top of the bridge so that the current passing through the filament, increases.

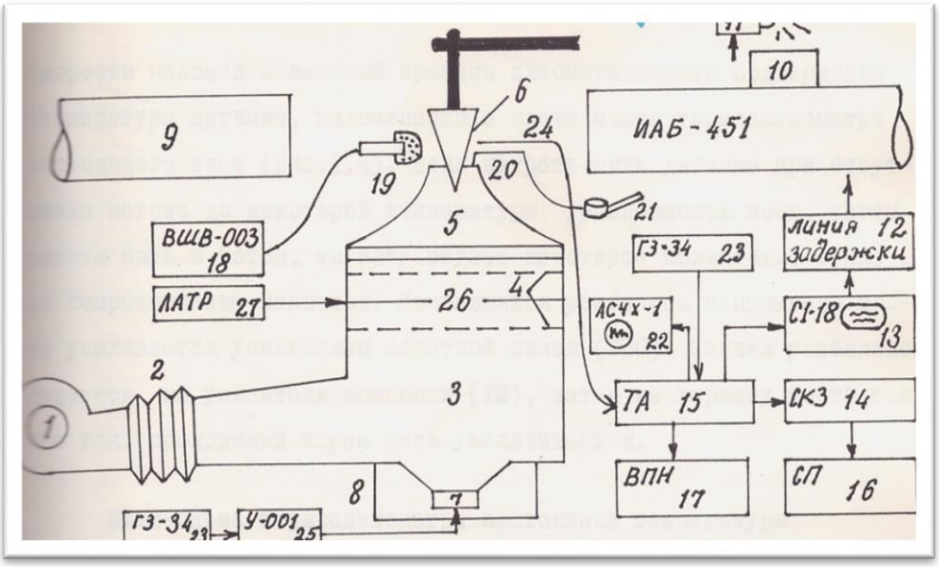

1-fan, 2- vibration damper , 3-soothing chamber, 4-grid alignment, 5- nozzle, 6- working medium, 7-speaker, 8- protective cover, 9- Tepler device , 10- focusing optics, 11- IFK lamp -120, 12- delay line, 13- oscilloscope, 14- SKZ voltmeter, 15- hot-wire anemometer, 16-recorder, 17-voltmeter of constant values, 18- sound level meter , 19-microphone, 20-pitot tube, 21-manometer MIN-240 , 22-frequency analyzer, 23-generator, 24- hot-wire anemometer probe, 25- amplifier, 26-heating grid, 27-transformer.

Fig. 4. Schematic diagram of an experimental setup for studying the vortex structure of a flow

In this case, the temperature of the thread and its resistance is restored, and the bridge is balanced. Thus, the bridge current is functionally related to the flow rate. In Figure 5: E is a constant voltage voltmeter for measuring the averaged speed, and$\sqrt{e^2}$ is a rms voltmeter for measuring the ripple of speed.

Data was recorded semi-automatically, i.e. the movement of the sensor was carried out using an engine mounted on the coordinator, and the output signals from voltmeters were fed to a two-coordinate recorder, type PDP4-002. For measurement, tungsten filaments with a diameter of 7 microns and a length of 3 mm were used.

The main technical characteristics of the hot-wire anemometer:

Frequency range 0-15 kHz

Resistance of the applied sensors 0,5-10 Om

Maximum output voltage 12 V

Diam etr threads of sensors 3-10 mk

Equivalent noise level in the 10 kHz

At a flow rate of 10 m / s 0.05%

A digital voltmeter for recording the average speed has an averaging interval of 1-100 s with a voltage measurement accuracy of 0.5%. The rms voltmeter (RMS) included in the set of the hot-wire anemometric system in the frequency range 3-155 kHz with an averaging interval of 3-30 s was measured with an accuracy of + -2.0%. When setting up the hot-wire anemometer and further monitoring its operation, the S8-13 oscilloscope was used. The frequency response of the spectrum of turbulent pulsations was measured by a spectrum analyzer of turbulent pulsations measured by a spectrum analyzer ASCH-1, which has an operating frequency band of 20–20 kHz.

2.3 Methods of measurement

When measuring the average velocity, static pressure, velocity pulsation, level of turbulence, friction coefficient on the wall and thermal characteristics of the jet, as well as a visual study of the vortex structure, we used the technique described in [38].

2.3.1 Methods of hot-wire anemometry

A heated filament hot-wire anemometer is used to measure flow velocity pulsations and has a high resolution.

For a thin filament, the length of which is large compared to its diameter, the temperature distribution along the filament is uneven and the measured resistance gives an average temperature along the length. There are two measurement methods: direct current method and constant temperature method. In the first, the current heating the thread is kept constant, which leads to pulsations in the temperature of the thread, due to the influence of the flow. In another, the heating current of the filament is controlled so that the released amount of heat ensures a constant filament temperature.

In practice, the thread is in an intermediate state when its temperature and heating current change slightly. However, they try to minimize the change in one of these parameters, and its influence is taken into account only in the form of an amendment.

A block diagram of the direct current method is shown in Figure 5. The essence of the method is as follows: the heated thread enters a resistive bridge, supplied with direct current. Under the influence of the flow velocity and the thread is cooled, a signal imbalance in the measuring diagonals ab resistance bridge. The signal is amplified by an amplifier with a frequency response in a special shape and operating at an average speed M meter. The ripple component is measured with a voltmeter of rms values of e^2. The disadvantage of this scheme is the drift of the amplifier and the errors associated with it when measuring average speeds.

Another variation of the direct current method is a carrier frequency system. The measuring bridge is powered by alternating current of increased frequency, which is selected in the range of 50-200 kHz. The measured signal is amplified by a strip force, detected, and its average value is recorded by the output meter M.

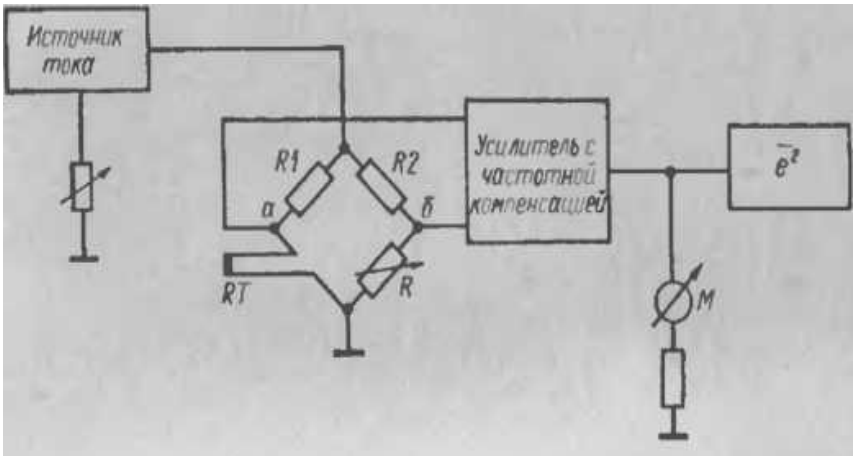

Fig. 5. Block - diagram of a direct current hot-wire anemometer

The pulsation component of the signal enters the amplifier with frequency compensation, at the output of which it is recorded using a rms voltmeter. This scheme has increased stability

when measuring average speeds, but it is quite complex and requires compensation for the capacitance of the measuring cable.

The simplicity of building electronic circuits operating by the direct current method has determined its significant distribution. The effect of thermal inertia on the measurement results.

The equation was obtained under the assumption of an ideal balance between the heat released during the passage of electric current and the heat transferred to the cooling stream, i.e., in the absence of thermal inertia of the filament. However, in reality, the heat capacity of the thread has a finite value, and therefore there is a certain delay period between the fast pulsations of the flow velocity and the corresponding pulsations of the temperature of the thread.

In this case, the thermal equilibrium of the filament at an arbitrary instant of time is described by equation (28):

$$\frac{I^2 R}{R - R_0} = A + B\sqrt{V} + C_T \frac{dT}{dt}, \tag{28}$$

where C_t is the heat capacity of the heated thread.

To analyze the effect of turbulence, suppose that $V = \overline{V} + \upsilon$, $R = \overline{R} + r$, $T = \overline{T} + \Delta t$.

Assuming that the intensity of turbulence is small, i.e., $\upsilon / \overline{V} \langle\langle 1$, and, therefore, $r / R_0 \langle\langle 1$, we obtain the relation between υ, r and Δt in the form of formula (29):

$$I^2 r = \left(A + B\sqrt{\overline{V}}\right) r + \left(\overline{R} - R_0\right) B\sqrt{\overline{V}} \frac{\upsilon}{2\overline{V}} + C_T \frac{d\Delta t}{dt}. \tag{29}$$

Since the resistance of the heated wire is $R = R_0(1 + \alpha\Delta t)$, then obviously $\Delta t = \frac{r}{R_0 \alpha}$,

where α is the temperature coefficient of resistance.

Substituting the value in equation (29), we obtain the formula in the form (30):

$$I^2 r = \left(A + B\sqrt{\overline{V}}\right) r + \left(\overline{R} - R_0\right) B\sqrt{\overline{V}} \frac{\upsilon}{2\overline{V}} + \frac{C_t}{2R_0} \frac{dr}{dt};$$

$$\frac{C_t}{2R} \frac{dr}{dt} + \left[\left(A + B\sqrt{\overline{V}}\right) - I^2\right] r = -\left(R - R_0\right) B\sqrt{\overline{V}} \frac{\upsilon}{2\overline{V}}; \tag{30}$$

Dividing the right and left parts of equation $\left[\left(A + B\sqrt{\overline{V}}\right) - I^2\right]$ (30) by term, we obtain equation (31):

$$M \frac{dr}{dt} + r = \upsilon N, \tag{31}$$

where $M = \frac{C_t}{\alpha R_0 \left[\left(A + B\sqrt{\overline{V}}\right) - I^2\right]}$; $N = \frac{\left(R - R_0\right) B\sqrt{\overline{V}} \frac{1}{2\overline{V}}}{\left[\left(A + B\sqrt{\overline{V}}\right) - I^2\right]}$.

Applying the Laplace transform [6] $d/dt = p$, we obtain equation (31) in the following form (32):

$$r(Mp + 1) = \upsilon N. \tag{32}$$

From where it is easy to obtain the transfer function of the link in the form of formula (33):

$$K(p) = \frac{r}{\upsilon} = \frac{N}{1 + Mp}. \quad (33)$$

The transition characteristic of this link is determined by a simple multiplication of expression (33) by *1 /p*, and as a result we obtain formula (34):

$$h(p) = \frac{N}{(1 + Mp)p}. \quad (34)$$

If we use the inverse Laplace transform and tables of operational relations, we can find the original image of equation (34).

Figure 6 shows the transient characteristics of the thread as an inertial link. If you draw a tangent to the transition characteristic curve at the origin, you can determine the time constant M of this link or determine as shown in Figure 6. To build the amplitude and phase characteristics of the link, we put $p = jw$ and substitute it into equation (33), as a result, we obtain expression (35) for the complex link transfer coefficient:

$$K(j\omega) = \frac{N}{1 + Mj\omega}. \quad (35)$$

From equation (35), you can determine the amplitude-frequency characteristic of the link in the form of formula (36):

$$K(\omega) = \frac{N}{\sqrt{M^2\omega^2 + 1}}. \quad (36)$$

Figure 7 shows graphs of the amplitude-frequency and phase-frequency characteristics of nitride (K_n, ϕ_n) and film (K_n, ϕ_n) sensors constructed according to equation (36). At a frequency w = 1/M, the amplitude-frequency response of the link begins to decline. Approximately 20 dB per decade, the magnitude of the phase shift tends to the value - π / 2.

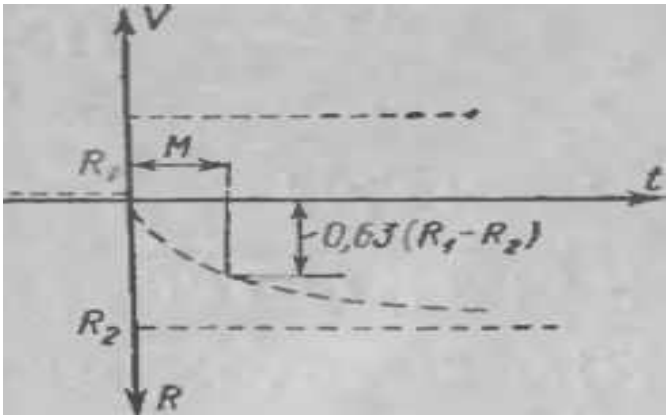

Fig. 6. The reaction of heated thermofilament (at constant current) to a sudden increase in flow rate

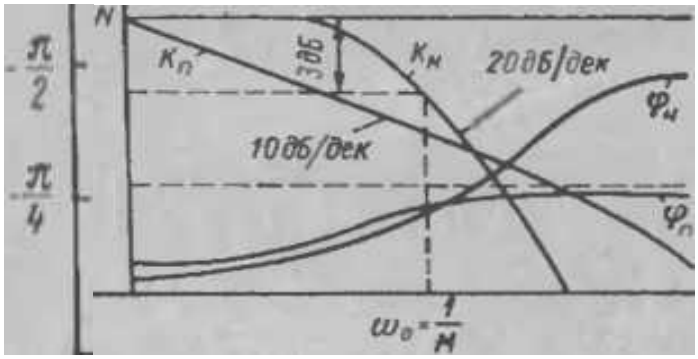

Fig. 7. The reaction of wire and film temperature sensors to a harmonic change in speed

From these graphs it can be seen that the signal taken from the filament at a frequency of w_0 begins to undergo amplitude and phase distortions due to the finite thermal inertia of the filament.

The experimentally recorded transition characteristics of filaments of different diameters allow us to conclude that for platinum filaments with a diameter of approximately 8 μm, w_o = 1800 Hz. Measurement of turbulent pulsations in a wider frequency range requires an amplifier with a special amplitude-phase-frequency characteristic.

The advantages of the constant temperature method: the ease of linearization of the output signal of the hot-wire anemometer, higher accuracy, the ability to measure large turbulence intensities, a large signal-to-noise ratio, and also the ease of adjusting the frequency response, attracted the close attention of investigators. Currently, the problem of instability of the feedback system is solved and almost all researchers use the constant temperature method.

A block diagram of the constant temperature method is shown in Fig .8. The essence of the method is as follows: a heat exchanger is included in one arm of the bridge of the resistance to the diagonal of the measurement, from which the differential amplifier is connected, including the voltage amplifier K_n and a current amplifier K_t.

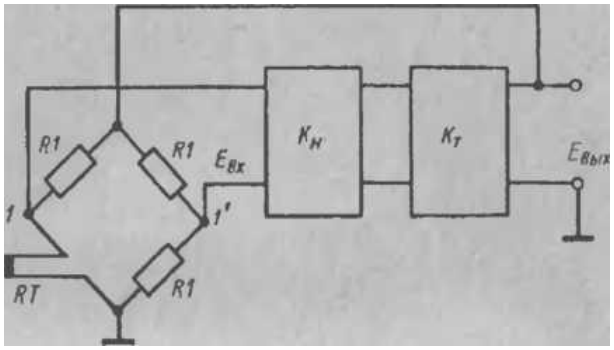

Fig. 8. Block diagram of a constant temperature hot-wire anemometer

The output of this amplifier is connected to the power diagonal of the resistor bridge. The electric current of the servo amplifier passes through the probe, whereby the wire or its film is heated to a certain temperature. The temperature of the heat exchanger is maintained by a servo-controlled system. The actual value of the consumed electricity is equal to the heat of the instantaneous heat for the environment. Heat losses depend on the temperature, pressure and speed of the measured medium, as well as on said inverter. If the temperature and pressure of the medium do not change during the measurement, the flow rate of the probe depends on the flow.

The principle used makes the anemometer especially suitable for measuring high-frequency flow pulsations. Without feedback, the upper frequency limit is reduced to approximately 100 Hz due to the influence of the probe capacitance; during the feedback, however, the frequency range increases with the feedback factor.

When the heat exchanger begins to cool due to the increase in flow, its resistance begins to change depending on the ratio $R — R_o = a(T - T_o)$.

A change in resistance leads to a change in the voltage drop between the diagonals of the *I-I '* bridge, which is fed to the input of the amplifier. This voltage is extended and directed to the bridge, increasing the current of the amplifier used to heat the light bulb and compensating for its cooling. The voltage E_o, which characterizes the heating of the sensor, is, therefore, a measure of the flow rate.

The feedback circuit consists of three parts: a temperature -sensitive transducer; a measuring bridge that responds to a change in the resistance of the thread and a feedback amplifier, the output of which is removed the power that is used to heat the sensor. An equation describing the dynamics of a system can be obtained by combining the basic equations describing each of its elements.

The power supplied for heating the filament, when using the equal-arm bridge, can be written in the form $\frac{E^2_{вых} R}{(R+R_1)^2}$. This power is consumed for heat transfer to the flow and the change in the temperature of the filament over time. In what follows, we assume that the heat transfer from the filament is a function of the flow velocity *F(u)* and is proportional to the temperature difference between the filament and the ambient air.

Denoting $\left[\left(A + B\sqrt{u}\right) = F(u)\right]$ in the King equation (37):

$$I^2 R = \left(A + B\sqrt{u}\right)\left(\overline{R} - R_0\right), \tag{37}$$

we get:

$$\frac{E^2_{вых} R}{(R+R_1)^2} - F(u)\frac{R-R_0}{\alpha} = C\frac{dR}{dt}. \tag{38}$$

The voltage at the input of the feedback amplifier is determined by the formula (39):

$$E_{вых} = \frac{E_{вых}(R_1 - R)}{2(R_1 + R)}. \tag{39}$$

For the gain of the feedback amplifier, the relation (40) is obtained:

$$M_1 \frac{d^2 E_{вых}}{dt^2} + M_2 \frac{dE_{вых}}{dt} + E_{вых} KE_{вх}, \tag{40}$$

where the time constants M_1 and M_2 take into account the presence of RC and LR circuits in the amplifier circuit, as well as imperfect frequency properties of the active elements of the circuit.

In a turbulent flow, the deviation of the values of E_{ex}, E_{VK} and R from their average value will be considered small, which will allow us to derive a linear dynamic equation of motion of the system. If derivatives of times and, in the equations (38) - (40) are zero, these equations constitute a system of static constant temperature anemometer, they hook it describe all the

characteristics in the case where a flow velocity fluctuations are absent. From these equations, we can find the dependence of the static value of E_o on u in the form of formula (41):

$$E_{вых} = \left[\frac{F(u)(\overline{R} - R_0)K^2(R_1 - \overline{R})^2}{R} \right]^{1/2}. \quad (41)$$

For large values of the gain, expression (41) is somewhat simplified to expression (42):

$$E_{вых} = \left[\frac{F(u)(\overline{R} - R_0)}{R} \right]^{1/2}. \quad (42)$$

In the turbulent flow there are fluctuations in velocity and the values of E_o, R, E_{VK} deviate from their average values. Of greatest interest are the equations for small deviations of e_o, r, e_{vc} from static values and formula (43) is derived:

$$\frac{E_{вых}}{4R_1^2}\left(r + \frac{4CR^2}{E_{вых}^2 \alpha}\frac{dr}{dt} \right) = \frac{dF(u)}{du}\frac{(R - R_0)}{\alpha} u \frac{2E_{вых}R}{4R_1^2} e_{вых}; \quad (43)$$

Equation (43) determines the relationship between the deviations of the variables of magnitude and their average values. This equation determine the dynamic characteristics of a constant temperature anemometer. You can get dynamic equation s feedback system (44):

$$\frac{E_{вых}}{4R_1^2}\frac{dF(u)}{du}u = e_{вых} + M'\frac{de_{вых}}{dt} + M'\frac{d^2e_{вых}}{dt^2} + M_1\frac{M}{K}\frac{d^3e_{вых}}{dt^3}. \quad (44)$$

Equation (44) is a third-order linear differential equation. As the gain increases, the coefficient MM_1 / K in this equation decreases.

If we assume that it is determined by the parameters of the amplifier and is a constant, then the time constant M, which characterizes the thermal inertia of the filament covered by feedback, can vary over a wide range by changing the gain of the feedback loop K.

The feedback system should be adjusted so that the optimal case of an a periodic solution of the differential equation (44) is realized. All other solutions to this equation lead to unstable operation of the feedback system.

As can be seen from equation (44), the time constant of the hot-wire anemometer M when working according to the constant temperature method is much smaller than for the direct current method. When the gain K of the feedback loop is of the order of 10-15 thousand, the frequency range of the constant-temperature anemometer is expanded to 30-50 kHz.

Due to the relatively small value of the time constant, the constant temperature method is suitable for measuring turbulent flows without the use of thermal delay compensation. Due to the constant temperature of the fiber, the constants A and B are constant, i.e. H. They are independent of turbulent pulsations. This is a significant advantage of the constant temperature method, where measurements must be performed on turbulent flows with high relative turbulence intensity [40].

2.3.2 Shadow and interference methods

About visualization fact: solid, placed in air flow, will provide it impacts, in turn angered the flow will be III Newton's law to provide the same effect on the body. From here two directions of research open.

It is first possible to examine the effect of the flow on the model, for example to measure the distribution of the normal pressure force acting on the body or to record the forces and

moments acting on the entire model. Second, we can examine the disturbed flow, namely: - give the nature, structure and location of these disturbances and the model strength. This type of testing is called model flow visualization. Ideally, to conduct an investigation of the aircraft properties required to load the registration model and visualize its flow, these investigations should be performed simultaneously. Tunnel tests without visualization - this is literally a study with your eyes closed.

Flow disturbances can be identified in different ways. The principle of operation of shadow and interference devices is based on the use of the same physical phenomenon - the reaction of a light beam to a change in the refractive index of a medium. The refractive index (n) only refers to its density according to the Gladstone - Dale formula: $k=(n-1)/\rho$, where k is a constant coefficient for a given gas and for a given wavelength .

For example, air at 0°C and $P=10^5$ Pa $k=0.22575$ for the yellow D - sodium line (l = 0.589 microns) dimension Density - g / cm ^{3}. It can be shown, that the measured value is a function of interferometer the refractive index of the medium n (x, y, z), obtained with the help of shadow devices - by the functions of the gradients of the refractive index $\left(\frac{\partial n}{\partial x};\frac{\partial n}{\partial y};\frac{\partial n}{\partial z}\right)$, and obtained with the help of direct - shadow settings - by the functions of the second derivative of the refractive index of the medium $\left(\frac{\partial^2 n}{\partial x^2};\frac{\partial^2 n}{\partial y^2};\frac{\partial^2 n}{\partial z^2}\right)$.

Direct shading method for flow visualization. The simplest method of visualization is the direct shadow method, in which another derivative of the refractive index of the device is recorded. A schematic of its application in a ballistic experiment is shown in Figures 9 and 10. Figure 9 shows a flow pattern around a cone and Figure 10 shows a stereo pair of sentinels.

The main elements that affect the visualization quality with this method are light sources for pulsed light. These images were obtained using a 1 ms spark source and an energy of about 1 J. The spark size was approximately 1 mm. This method works well under normal atmospheric conditions.

Visualization using shadows. A shielding series device is often used in the wind to look at supersonic and transonic currents, for example, IAB 451 with a visualization field with a diameter of 230 mm produced by the Kazan Optical and Mechanical Plant. The scheme of a shadow device operating according to the Tepler method is presented in Figure 11.

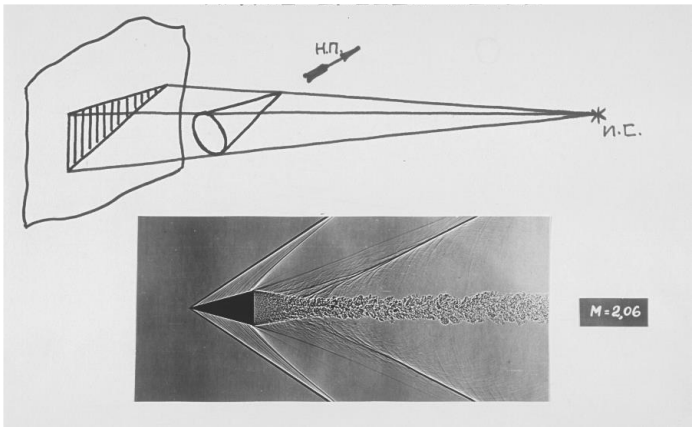

Fig. 9. Direct shadow method of visualization of currents. Cone wrap pattern

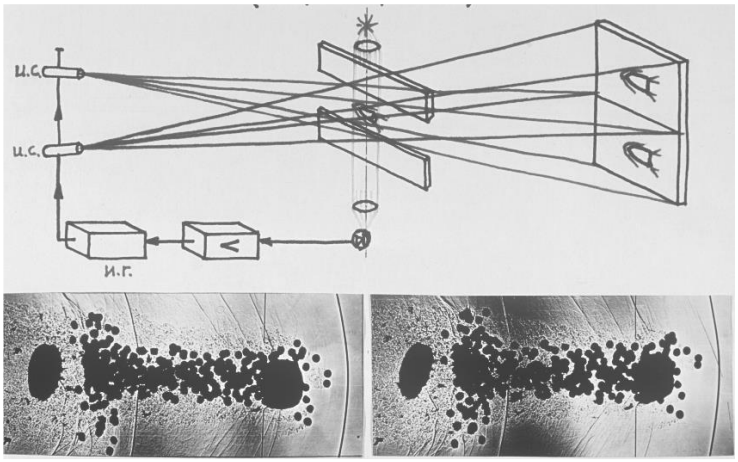

Fig. 10. Direct shadow method of visualization of currents. Stereopair shot from a shotgun

To isolate the flow structure, a small light source is required, his is achieved by focusing the trace image of the lamp (1) on the light curtain (3). Aimed at the capacitor lens (2). The standard membrane is a groove, the size of which is regulated by a micrometer screw. The volume of the examined room is illuminated by a parallel beam of light from the opening. The beam can be shaped either by a lens system such as Tepler or by a mirror system as described in IAB 451 (Fig. 11). After the functional part of the wall tunnel (5) has passed through the test object (6), the rays are directed to the receiving part of the optical system (lens or mirror). Near this focus is the imaging diaphragm (7) - the Foucault knife.

When passing the object (6), the parallelism of the rays is violated due to a change in the refractive index. For example, by changing the position of the Foucault knife, it is possible to remove directional rays from one angle or another from the light beam. In addition, in the plane of the image 9 forming the lens 8, the areas which caused the air to be reflected are scored. The visualization scheme can be not only the sharp edge of the knife, but also other devices such as a wall, and so on. Examples of images obtained using a shadow device with a lens system and various visualizing diaphragms are shown in Figures 12, 13.

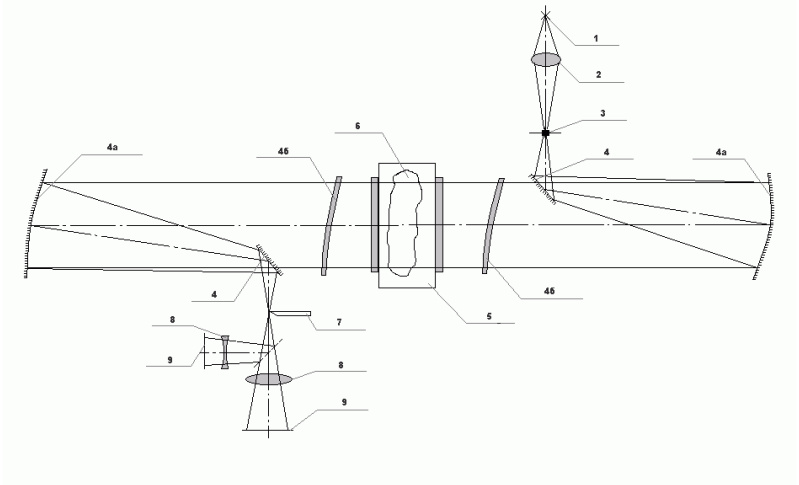

1 — light source, 2 — condenser , 3 — illumination diaphragm , 4 a — surface element of a spherical mirror , 4 b — meniscus to compensate for aberrations of the spherical mirror , 5 — working part of the wind tunnel, 6 - the investigated object , 7 - imaging diaphragm (Foucault knife), 8 - lens, 9 - screen .

Fig. 11. Scheme of a shadow device operating according to the Tepler method

Figure 12 shows the flow around the pointed cylinder and the axisymmetry of the egg inlet; Figure 13 shows the flow around the profile at different positions of the visualizing thread. The method is rightly classical and is widely used in aerodynamic experiments.

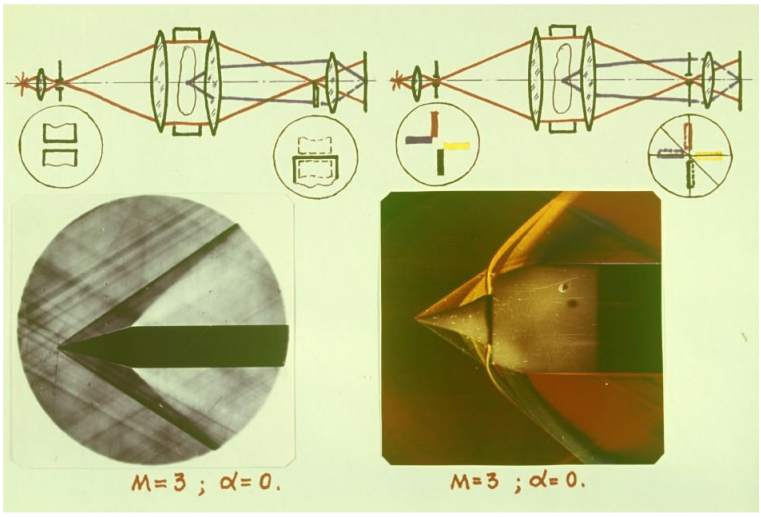

Fig. 12. Flow around the pointed cylinder and the axisymmetry of the egg inlet

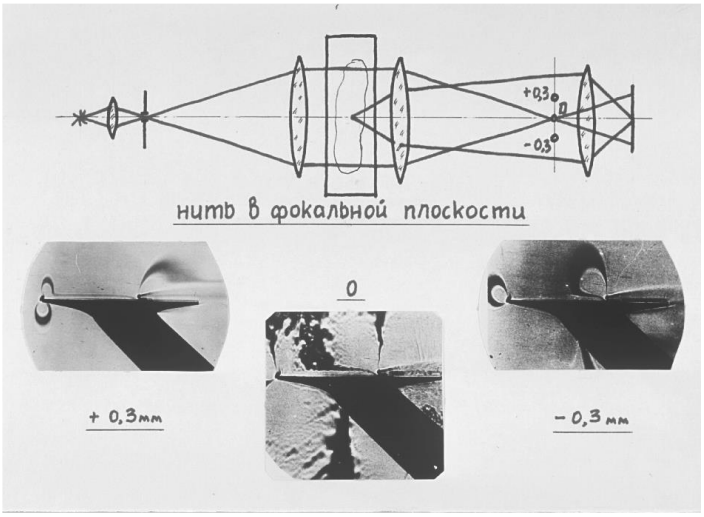

Fig. 13. Flow around profile at various positions of an imaging filament

Interferometer Mach - Zehnder interferometer. In a classical interferometer, a superposition of two light fluxes occurs, one of which passes through the studied region, and the other is the reference one. The scheme of such an interferometer and the results are presented in Fig. 14. The disadvantage of this scheme is the significant vibration sensitivity and the large weight of the system (about 1000 kg), which excludes its mobile use.

Shear interferometer. These shortcomings are deprived of the shear interferometer developed by the State Optical Institute. Academician S.I. Vavilov (GOI). The circuit device and its external view presented in Figure 15.

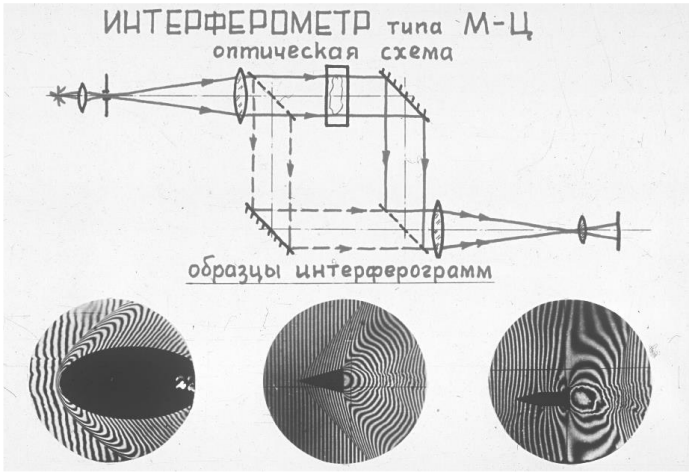

Fig. 14. Scheme of the Mach - Zehnder interferometer

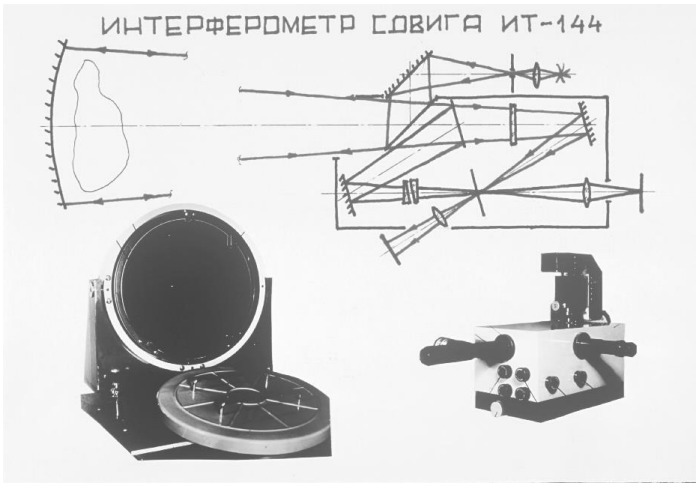

Fig. 15. Scheme of the interferometer shear

The universal shear interferometer (approximately 250x250x400 mm) is intended to study the transparency of homogeneity in solid, liquid and gaseous media, to study the quality of spherical concave and spherical surfaces and, in particular, to study large fields gas dynamics. Interference in this diagram is achieved by overlapping two light fluxes that flow homogeneously but are laterally shifted relative to each other. The amount of compensation can vary greatly. The results of using a shear interferometer are shown in Figure 16. The device operates in the main version of the system with a spherical mirror with a diameter of 500 mm and a radius of curvature R = 5000 mm. The spherical mirror and the device itself were mounted on both sides of the active part of the wind tunnel on separate non-cushioned bases.

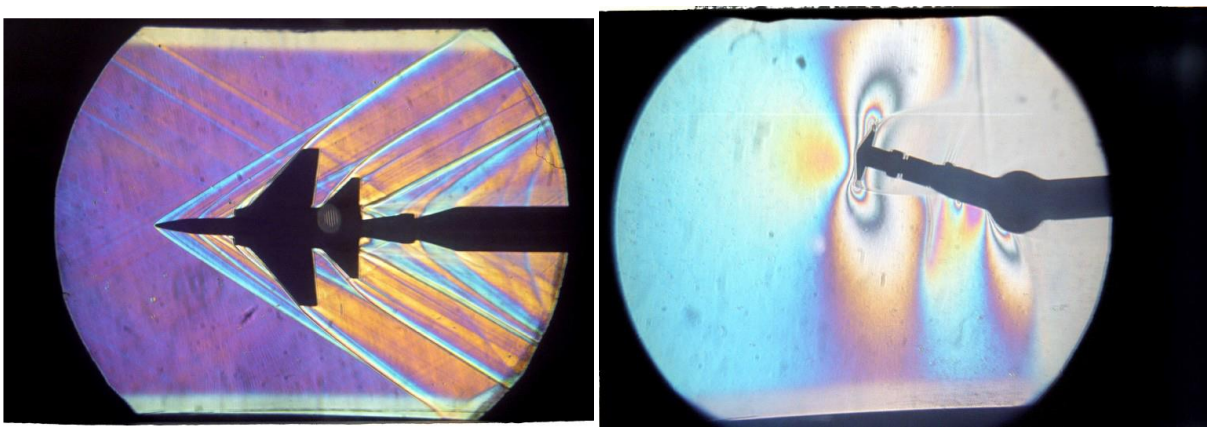

Fig. 16. Results of using a shear interferometer

2.3.3 Visualization of large-scale vortex structures in a turbulent jet

Photo and video registration of a clean jet and a jet excited by a harmonic acoustic signal was carried out in an acoustic damped chamber measuring 10 x 5 x 4.7 m^3. We studied a cold jet flowing out of a conical nozzle with a diameter of 4 cm at a speed of 40-140 m/s (M = 0.12 ... 0.42). In some experiments, the jet velocity was 200 m/s. A source of longitudinal acoustic excitation was a loudspeaker. The frequency of acoustic excitation f_{ex} varied in the range of 600-2500 Hz. To isolate large-scale vortex structures in a jet against the background of uncorrelated small-scale pulsations, a method was used that can be called the optical averaging method. The image of the investigated part of the jet is repeatedly exposed to the same frame, while repeating events are highlighted, and random ones are smoothed out. Registration was carried out in transmitted light using a shear interferometer. The light source was pulsed, operating in the strobe mode, with a frequency of light pulses that can be smoothly changed in the range 0 - 300 Hz. The frequency of light stroboscopic pulses $f_s = f_{ex/n}$ *was* chosen as high as possible so that the condition $f_s \leq 300$ Hz was fulfilled. At this frequency periodical occurring events in the same place jet (here are periodically formed in the initial section of the jet vortex rings) are repeatedly exposed to a single frame, and a slight misalignment frequency strobe and irradiation frequency can achieve the effect of high-speed video with respect to repetitive events.

Figure 17 presents video frames excited jet at different speeds expiration obtained by stroboscopic light and tuning the interferometer to a horizontal shift of the wave fronts. With the interferometer of translations ha was registered dynamic motion separate vortex rings in the air (Figure 18).

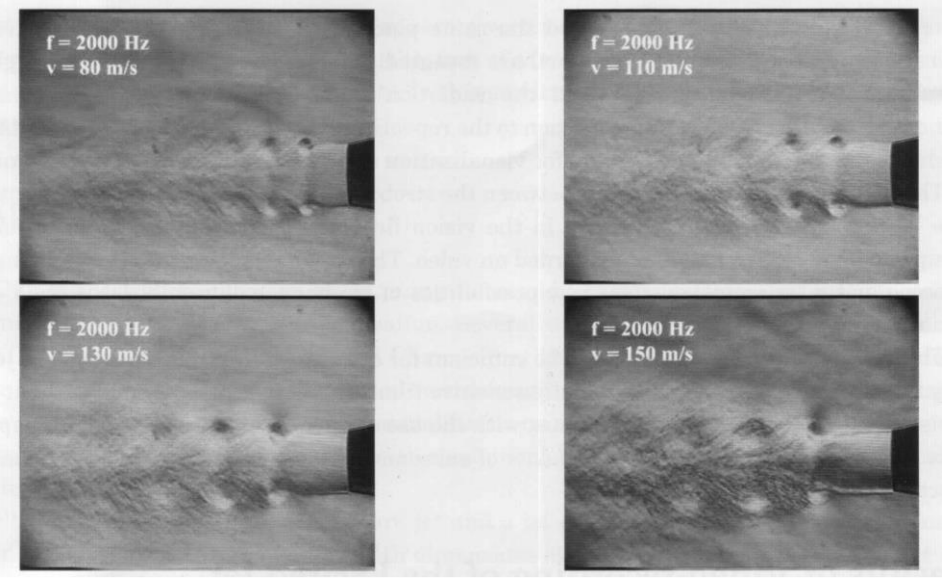

Fig. 17. In the video cadres of an excited jet at various flow rates obtained under stroboscopic illumination

Shadow and interference methods are still a reliable means of visualizing currents. In particular:

- The direct shadow method is the easiest method to observe shock waves at normal pressure and temperature.

- The classic Tepler method with multiple visualization membranes reliably differentiates optical homogeneities over a wide range of gas densities, but due to their properties and the size of the properties, the device that carries out this method is stationary.

- The visualization system with shear interferometer enables the visualization and qualitative analysis of two-dimensional subsonic flows around models with a free flow speed of 20 m / s without local heating along the light beam path in the zone. inhomogeneous ~ 2 m.

- The use of a shear interferometer in combination with flash lighting made it possible to identify the dynamics of coherent structures in the flow.

- The latter system can work in a mobile version [41].

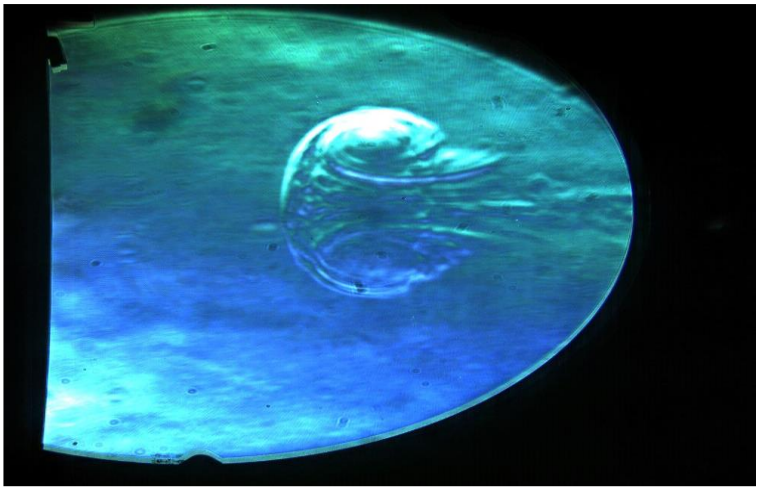

Fig.18. The dynamics of the motion of an individual vortex ring in air, recorded using a shear interferometer

2.3.4 Measurement of average speed, static pressure and friction stress on the wall

To determine the average speed at a fixed point, a full pressure Pitot tube with an external tip size of 0.1 x 1.0 mm and a wall thickness of 0.05 mm was used. A tube with a flattened end was previously calibrated on a wind tunnel with a Pitot tube with a circular cross-section of 1 mm in diameter. The formula for calculating the speed from the pressure gauge is found from the equilibrium condition of the total flow pressure and pressure in the manometer, i.e. $(-\rho u^2)/2+p_{st} = p$, whence formula (45) is derived:

$$u=\xi\sqrt{2(p-p_{cm})/\rho}, \quad (45)$$

where ξ is the calibration coefficient, $\rho = (\rho_0 \cdot p \cdot T_0 / p_0 \cdot T)$ is the air density, $\rho_0 = 1.293$ kg/m^3, $p_0 = 760$ $mm\ Hg.$, $T_0 = 273$ K, p and T - pressure and absolute temperature in the conditions of the experiment.

The value of static pressure was calculated by the formula (46):

$$\Delta P = P - P_0 = k \cdot \Delta h, \quad (46)$$

where Δh is the height of the liquid in the pressure gauge tube; k is the inclined coefficient of the micromanometer.

The surface friction coefficient was measured using Preston tubes [42] and the Clauser method [43] . It can be represented as formula (47):

$$c_f = 2 \cdot \tau_w / \rho u_m^2, \quad (47)$$

τ_w is the friction stress on the wall,

u_m is the maximum velocity on the axis of the jet in this section.

The influence of the velocity gradient and the proximity of the wall on the readings of the total pressure tube when measuring surface friction and the velocity distribution in the turbulent boundary layer was taken into account.

2.3.5 Measurement of the pulsation component of the velocity and frequency response of coherent structures

The values that determine the flow turbulence are of a statistical nature, at each point the values pulsate. Pulsating are speed, pressure, temperature, density and other parameters of the jet. Let us describe the methodology for measuring the velocity pulsation; the actual value of the pulsating velocity at a given time is represented as the sum (48) of its velocity $\bar{u}$ and the pulsating component u'.

$$u = \bar{u} + u', \quad (48)$$

at voltages: $E = \bar{E} + \sqrt{l'^2}$, (49)

where $\sqrt{l'^2}$ is the rms velocity value.

With the heat balance between the filament of the hot-wire anemometer and the environment moving at a speed u, the following relation holds (50):

$$E^2 = E_0^2 + B\sqrt{u}. \quad (50)$$

Here E_0 is the output voltage of the hot-wire anemometer in the absence of flow,

E - current voltage in the presence of flow.

Solving equations (48), (49), (50) together and taking into account that $u' << \bar{u}$ we obtain the final formula (51) for calculating the relative level of turbulence as proposed in [44].

$$\varepsilon = \frac{\sqrt{\overline{u'^2}}}{\bar{u}} = \frac{4E\sqrt{l'^2}}{\bar{E}^2 - E_0^2}. \quad (51)$$

To determine E, it is necessary to calibrate the dependence $E=f(u)$, i.e. a hot-wire anemometer sensor with a Pitot tube in a uniform flow. When extrapolating the calibration curve of the point, where $u=0$, corresponds to the value of E_0. The value of the intensity of the velocity pulsations, referred to the flow velocity at the nozzle exit u_0, can be calculated by the formula (52):

$$\varepsilon = \frac{\sqrt{\overline{u'^2}}}{\overline{u}} = \frac{4E\sqrt{l'^2}}{\left(\overline{E}_{и}^{\,2} - E_0^2\right)^2}, \tag{52}$$

where E_n - the value of the output voltage of the hot-wire anemometer, corresponding to the value of the velocity at the exit of the nozzle. The value of the average velocity related to the jet velocity at the exit of the nozzle is determined as follows (53):

$$\frac{u}{u_0} = \left(\frac{E^2 - E_0^2}{E_{и}^2 - E_0^2}\right)^2. \tag{53}$$

The frequency of natural vortex formation in the initial section of the jet was determined from the spectrum of velocity pulsations, which was measured by the ASCH - 1 analyzer and recorded by the PDP4-002 recorder.

The analyzer reading was previously calibrated using the GZ-34 signal generator.

When measuring the spectra in a free bias layer, a hot-wire anemometer sensor was installed in the region of the onset of disturbances in the shadow flow pattern. Then, after installing the sensor, the jet heater was turned off, and the spectrum was recorded in the absence of heating.

The degree of periodicity of the flow can be characterized by the value F(f), which is defined as (54):

$$F(f) = \int_{0.95f}^{1.05f} l(f)df \div \int_{0}^{\infty} l(f)df, \tag{54}$$

where $l(f)$ is the voltage ripple spectrum of the output signal of the hot-wire anemometer, f *is the* frequency of the maximum of the spectrum (characteristic frequency).

2.4 Measurement errors

Since the measurements used tools, instruments, apparatus and measurement procedures that are traditionally used in aerodynamic experiments, we restrict ourselves to providing data on the errors associated with the features of our plants. Random errors or the degree of reproducibility of the experiments were determined by the direct measurement method, and the total error by the method of indirect measurements [45]. Below are the total errors corresponding to the average values of the measured value. The errors in measuring the average speed by the full pressure tube are mainly due to the velocity gradient and proximity of the wall, and the static pressure, when measuring the static pressure by the tube, is not parallel to the streamline to the surface of the cone. The presence of significant errors in the measurement of velocity pulsations by the hot - wire method is caused, first of all, by the difference in the calibration coefficient of the sensor from 0.5 and the special sensitivity of the sensor to external influences. The imperfections of the Preston and Clauser methods in determining the local friction stress on the wall make us speak of its approximate value, the error in the heat flux density q_w *is* affected by heat loss due to heat conduction and the difference in the

temperature of the jet at the nozzle exit and the environment, the unevenness of heating, and also the error when determination of electrical power.

The total errors of the quantities determined in the experiments are shown in Table 1. The geometric and operational parameters of the experimental studies are summarized in Table 2.

Table 1 – Total relative errors

Measured variable or device	Measurement error or accuracy	to what extent were measurements taken
Coordinate, mm	0,02	
б, mm	0,1	(2,5÷10,0)mm
R, mm	0,1	(7,5 ÷230) mm
S_R ,%	0,25	0,0087 ÷ 0,577
w ,min	1,0	(0÷ 90)°
u, %	0,5	(3 ÷ 80) m/s
T_u ,%	12,0	(0 ÷ 30) %
q,%	5,0	
α, %	6,0	
Voltmeter V7-21, V	0,001	
Voltmeter D5015 accuracy class	0,2	
Voltmeter D50040 accuracy class	2	
Ammeter arrow. accuracy class	0,5	
f, Hz	0,5	
Current transformer UTT-6M1, accuracy class	0,2	

Table 2 – Geometric and operational parameters of the study

б, mm	S_R	w, grad	u_0 , m/s	What is measured
3,0; 4,0; 5,0	0,299;0,338;0,455	15°	30,0; 40,0; 50,0; 60,0	Medium Speed Profiles
3,6; 4,0; 5,0; 7,5	0,045; 0,182; 0,238; 0,405	30°	30,0; 40,0; 50,0; 60,0	
5,0	0,455	15°	40,0; 50,0	Ripple velocity profiles
5,0	0,238	30°	30,0; 40,0; 50,0	
5,0	0,710	15°	3÷ 35	Vortex frequency, pulsation spectra

3 Results of the study of aerodynamics of a radial jet and a jet extending along the cone

3.1 An approximate calculation of a turbulent jet propagating along a cone

An approximate calculation of a turbulent jet propagating along a conical surface can be carried out by the method of integral relations. The results of the study are given in application A. Usually, in theoretical calculations of wall jets, velocity profiles in the wall and outer boundary layers of the jet are specified. In this case, to the maximum speed, the profile is set in the form of a power law (55):

$$\frac{u}{u_m} = \left(\frac{y}{\delta_m}\right)^n , \qquad (55)$$

where, unlike the boundary layer of a uniform flow,

$n = \frac{1}{12} : \frac{1}{14}$, whereas for the same numbers $Re \approx 10^5$ for a homogeneous flow $n = \frac{1}{7}$. The velocity profile in the outer layer is considered to coincide with the profile of the free jet. The paper [13] has been proposed semiempirical form la (56):

$$\frac{u}{u_m} = f(\eta) = 1.426\eta^{\frac{1}{8}}(1 - 503 \cdot \eta)^{\frac{3}{2}}, \qquad (56)$$

satisfactorily describing velocity profiles for all semi-limited turbulent jets (Figure 19).

Here $\eta = \frac{y}{\delta_{0.5}}$. According to this formula, the thickness of the inner boundary layer is $\delta_m = 0.153\delta_{0.5}$, and the total thickness of the jet is $\delta_0 = 1.989$.

Note, however, that the relationship $\delta_m = 0{,}153\ \delta_{0.5}$ is approximate, the value of δ_m depends on the Reynolds number, and the ratio $\frac{\delta_m}{\delta_{0.5}}$ is a weak function of the Reynolds number and distance x [15].

Using formula (56), we can solve the problem of a turbulent jet propagating along a cone by the method of integral relations taking into account the finite value of friction on the wall.

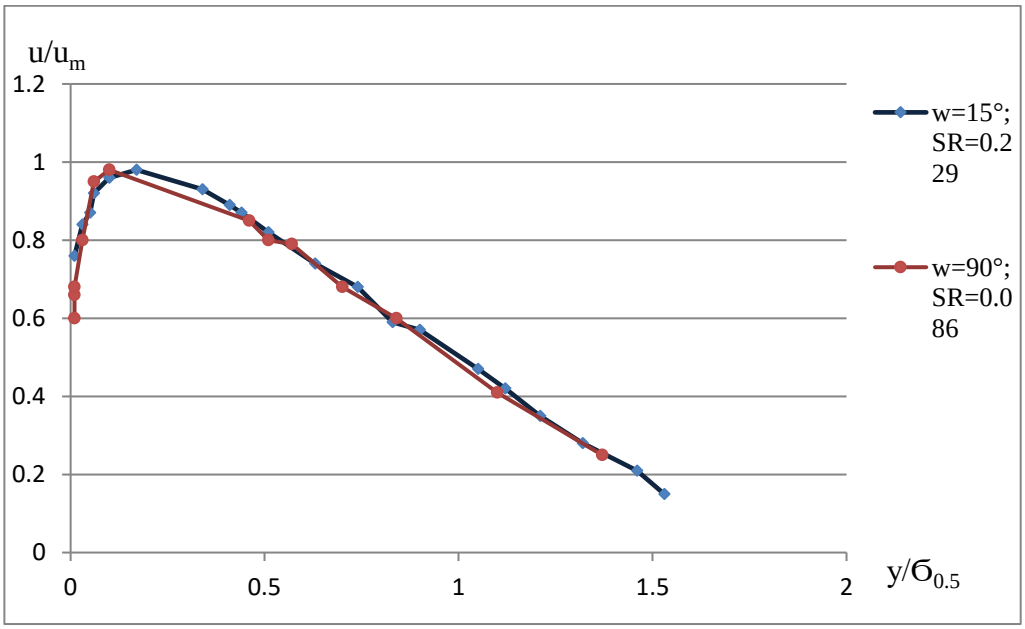

Fig. 19. Dimensionless velocity profiles of semi-limited jets

Consider a cone with a semi-angle at the vertex *w* and a smooth hydraulic surface. Let a turbulent stream propagate along the surface of the cone towards the base from a ring source located on the surface of the cone in a certain section with radius *R* (Figure 3).

The coordinate origin is located at the nozzle exit, the *x* axis is directed along the generatrix of the cone in the direction of the jet, and the *y* axis is perpendicular to the cone surface. The equation of motion of a turbulent semi-limited jet in the selected coordinate system has the form (57):

$$u\frac{\partial u}{\partial x}+\vartheta\frac{\partial u}{\partial y}=\frac{1}{\rho r}\frac{\partial(\tau\cdot r)}{\partial y}, \tag{57}$$

continuity equation (58):

$$\frac{\partial(ru)}{\partial x}+\frac{\partial(r\vartheta)}{\partial y}=0, \tag{58}$$

where *u* and are the velocity projections on the *x* and *y* axes, respectively , ρ is the fluid density, τ is the shear friction stress, *r* is the distance from the flow point under consideration to the cone axis.

As can be seen from Figure 3, we can obtain (59):

$$r=r_0(x)+y\cos\omega=R\pm x\sin\omega+y\cos\omega \tag{59}$$

where $r_0(x)=R \mp x\,sinw$ - radius , the section under consideration of the cone. The *"+"* sign refers to the case of the jet spreading towards the base , *" -"* - to the case of flow towards the top.

The boundary conditions are specified in the form (60):

$$u=\vartheta=0 \quad \text{at } y=0$$
$$u=0 \quad \text{for} \quad y=\delta_0 \tag{60}$$

Since for a turbulent semi-bounded source jet it is impossible to obtain invariants similar to the invariant for a laminar jet, it is necessary to set the maximum velocity in a certain section *x* , i.e. put $u_m = u_{m0}$ for $x = x_0$.

We set the velocity profiles and the friction stress along the jet cross section and determine the jet development with distance from the nozzle. By analogy with the laminar flow, the friction stress is usually set in the form (61):

$$\tau=(\mu+\varepsilon)\frac{\partial u}{\partial y}, \tag{61}$$

where μ is the dynamic viscosity coefficient, ε is the apparent turbulent viscosity.

In problems of free turbulent jets, it is assumed that ε is constant over the cross section and varies along the jet. However, this assumption is not valid for a semi-limited jet, where near the wall ε decreases to zero. By - apparently jet ε is also reduced at the external border in view of the fact that the jet velocity drops to zero and again goes over to laminar.

Therefore, the friction stress in the cross section of a semi- limited jet can be represented in the form (62):

$$\tau=c_1\rho u_m\delta\eta^{\frac{7}{8}}(1-0.503\eta)\frac{\partial u}{\partial y}, \tag{62}$$

where $c_1(R_l)$ is some function $R_l(R_l = \frac{u_m\delta}{\nu})$, determined from experience. Substituting in (62) the velocity value from (56) we obtain the formula (63):

$$\tau = \frac{1}{2} c_f \rho u_m^2 (1 - 6.535\eta) \cdot (1 - 0.503\eta)^{\frac{3}{2}}, \tag{63}$$

where $c_f = \frac{\tau_w}{\rho u_m^2} = 0.3564 \cdot c1$ is the coefficient of friction on the wall.

To solve the problem to the end, it is necessary to determine the dependences of δ and u_m on x. For this, we distinguish two integral relations from the equations of motion.

Multiply equation (57) by r, (58) by u and add. Integrating the obtained expression over y within the limits of $(0, \delta_0)$, we obtain the first integral relation (64):

$$\frac{d}{dx}\int_0^{\delta_0} ru^2 dy + \frac{1}{\rho} r\tau_w = 0. \tag{64}$$

We multiply equation (57) by $2u \cdot r$, equation (58) by u^2 and add them. Integrating the obtained expression over y within the limits of (o, δ_0), we obtain the second integral relation in the form (65):

$$\frac{d}{dx}\int_0^{\delta_0} ru^3 dy + \frac{2}{\rho}\int_0^{\delta_0} r\tau \frac{\partial u}{\partial y} dy = 0. \tag{65}$$

Substituting into equations (64) and (65) the velocity values from (56) and the friction stress from (63), we obtain the expression (66), (67):

$$\frac{d}{dx}\left\{(R \pm x\sin\omega) u_m^2 \delta_{0.5} \int_0^{\eta_0} f^2 d\eta + u_m^2 \delta_{0.5}^2 \cos\omega \int_0^{\eta_0} \eta f^2 d\eta\right\} + \frac{1}{\rho}(R + \sin\omega)\tau_w = 0 \tag{66}$$

$$\begin{aligned} &\frac{d}{dx}\left\{(R \pm x\sin\omega) u_m^3 \delta_{0.5} \int_0^{\eta_0} f^3 d\eta + u_m^3 \delta_{0.5}^2 \cos\omega \int_0^{\eta_0} \eta f^3 d\eta\right\} + \\ &+ c_f u_m^3 (R \pm x\sin\omega)\int_0^{\eta_0} g \frac{\partial f}{\partial \eta} d\eta + \delta_{0.5} c_f u_m^3 \cos\omega \int_0^{\eta_0} g \cdot \eta \frac{\partial f}{\partial \eta} d\eta = 0 \end{aligned} \tag{67}$$

where $g(\eta) = (1-6.355\eta)(1-0.503\eta)^{3/2}$, $\eta_0 = \frac{\delta_0}{\delta_{0.5}} = 1.989$ and $f(\eta) = \frac{u}{u_m}$;

Unfortunately, the system of equations (66) and (67) in a general form is not analytically solved. Therefore, we consider the limiting case when there is an expression (68):

$$\delta_{0.5} \cdot \cos\omega \langle\langle R \pm x\sin\omega. \tag{68}$$

This condition is valid for a sufficiently large opening angle of the cone and a large radius of its cross section at the location of the nozzle. Then, substituting the numerical values of the integrals, we transform these equations to the form (69):

$$\left.\begin{aligned} 1.483\frac{1}{r_0}\frac{dr_0}{dx} + 2.967\frac{1}{u_m}\frac{du_m}{dx} + 1.483\frac{1}{\delta_{0.5}}\frac{d\delta}{dx} + \frac{c_f}{\delta_{0.5}} = 0 \\ 0.259\frac{1}{r_0}\frac{dr_0}{dx} + 0.778\frac{1}{u_m}\frac{du_m}{dx} + 0.259\frac{1}{\delta_{0.5}}\frac{d\delta}{dx} + \frac{c_f}{\delta_{0.5}} = 0 \end{aligned}\right\} \tag{69}$$

Subtracting them one from another, and integrating, we obtain (70):

$$\delta_{0,5}(R \pm x\sin\omega)u_m^{1.79} = A = const. \quad (70)$$

Expressing $\delta_{0.5}$ from (70) and substituting into the first equation (69), after integration we find for $c_f = const$ and we obtain formula (71), (72):

$$\frac{u_m}{u_0} = \left[\frac{A}{5.69c_f Rx \pm \frac{1}{2}x^2\sin\omega}\right]^{0.56} \quad (71)$$

$$\delta_{0,5} = 5.69c_f \frac{Rx \pm \frac{1}{2}x^2\sin\omega}{R \pm x\sin\omega}; \quad (72)$$

when $c_f = \frac{K}{\frac{u_m x^{0.2}}{\nu}}$ we obtain the expressions (73) and (74):

$$\frac{u_m}{u_0} = \frac{0.31\cdot A^{0.63}}{K^{0.63}} \cdot \frac{\mathrm{Re}_0^{0.13}}{(x/\sigma)^{0.504}\cdot(1 \pm 0.445\frac{x}{R}\sin\omega)^{0.63}}; \quad (73)$$

$$\frac{\delta_{0.5}}{\sigma} = \frac{7.98\cdot K^{1.13}}{A^{0.13}\cdot \mathrm{Re}^{0.22}} \cdot \frac{(x/\sigma)^{0.504}\cdot(1 \pm 0.445\frac{x}{R}\sin\omega)^{1.13}}{1 \pm \frac{x}{R}\sin\omega}; \quad (74)$$

Here A is the integration constant, k is the proportionality coefficient.

As will be shown in the following, the results of experiments according to formulas (73) and (74) are in better agreement with the results of experiments at large angles of opening of the cone. It qualitatively correctly shows the nature of the change in the thickness of the jet with distance from the nozzle in the jet, propagating towards the top of the cone. At the same time et and the formula effect assumptions (68) along a poor description of the jet cone with a small opening angle and at low values of R. Therefore, for a satisfactory description of the results of the experiments need to use semi-empirical formulas, unifying the results of (73), (74), as well as experimental data.

An analysis of the experimental data on the change in the thickness of the diverging jet and the jet along the plate and cylinder shows that all of them are described by one regularity (75):

$\Delta_{0,5}$=0.070x (75)

If this expression is substituted into equations (66) and (67), we can obtain integral relations in the form (76), (77):

$$\frac{d}{dx}\left\{0.0519(R \pm x\sin\omega)xu_m^2 + 0.00172u_m^2x^2\cos\omega\right\} + \frac{c_f}{2}(R \pm x\sin\omega)u_m^2 = 0; \quad (76)$$

$$\frac{d}{dx}\left\{0.0426(R \pm x\sin\omega)xu_m^3 + 0.00129u_m^3x^2\cos\omega\right\} + \quad (77)$$
$$+ 2.344(R \pm x\sin\omega)c_f u_m^3 + 0.0943c_f u_m^3 x\cos\omega = 0.$$

Taking the derivatives of (76) and (77) with respect to x, substituting the value of c f from the first integral condition into the second, we obtain the following differential equation (78) with separated variables and:

$$\frac{du_m}{u_m} = -\frac{0.559R^2 + (1.667R\sin\omega + 0.0650R\cos\omega)x + (1.118\sin^2\omega + 0.0922\sin\omega\cos\omega + 0.0183\cos^2\omega)\cdot x^2}{R^2 + (2R\sin\omega + 0.0887R\cos\omega)x + (\sin^2\omega + 0.0887\sin\omega\cos\omega + 0.00183\cos^2\omega)\cdot x^2} \cdot \frac{dx}{x}. \quad (78)$$

The solution of equation (78) leads to formula (79) for changing the maximum speed of diverging conical and radial jets, as well as jets propagating over the surface of a flat plate and a round cylinder, taking into account the influence of the transverse curvature parameter, the taper angle, and the initial Reunolds number in the following form:

$$\frac{u_m}{u_0} = \frac{1}{\left[1+\left(\frac{x/\sigma+2}{4.88\,\mathrm{Re}^{0.11}}\right)^4\right]^{0.14}}\left[\frac{1+(\sin\omega+0.0428\cos\omega)\cdot S_R\cdot\frac{x_н}{\sigma}}{1+(\sin\omega+0.0428\cos\omega)S_R\frac{x}{\sigma}}\right]^n \cdot$$

$$\cdot\left[\frac{\sin\omega+0.0210\cos\omega+(\sin\omega+0.0428\cos\omega)^2 S_R\frac{x}{\sigma}}{\sin\omega+0.0678\cos\omega+(\sin\omega+0.0428\cos\omega)^2 S_R\frac{x}{\sigma}}\cdot\frac{\sin\omega+0.0210\cos\omega+(\sin\omega+0.0428\cos\omega)^2 S_R\frac{x_н}{\sigma}}{\sin\omega+0.0678\cos\omega+(\sin\omega+0.0428\cos\omega)^2 S_R\frac{x_н}{\sigma}}\right]^N, \quad (79)$$

where $n = 1.118\cdot\left(\frac{\sin\omega+0.0405\cos\omega}{\sin\omega+0.0428\cos\omega}\right)^2 - 0.559$

$$N = \frac{0.427(\sin^3\omega + 0.774\sin^2\omega\cos\omega + 0.0417\sin\omega\cos^2\omega + 0.0076\cos^3\omega)}{\cos\omega(\sin^2\omega + 0.0887\sin\omega\cos\omega + 0.00183\cos^2\omega)}. \quad (80)$$

3.2 The influence of the parameter of transverse curvature, taper angle and direction of the outflow of the jet on the development of the boundary layer

In the experimental setup described in the second chapter, the basic hydrodynamic parameters of a semi-limited jet propagating over the surface of a cone and disk were investigated. The main operational and geometric flow conditions are given in table 1.

The results of measurements of the velocity profiles in the cross sections of the main section of the jet are shown in Figures 19, 20, 21. As can be seen from Figure 19, the velocity profiles in coordinates$\frac{u}{u_m} = f(\frac{y}{\delta_{0.5}})$ for all the considered modes are almost self-similar.

Figure 21 shows the results of measurements of velocity profiles in the initial, transitional, and main sections of the conical jet at $\omega = +30°$, where qualitative and quantitative the difference between diverging and converging semi-limited jets.

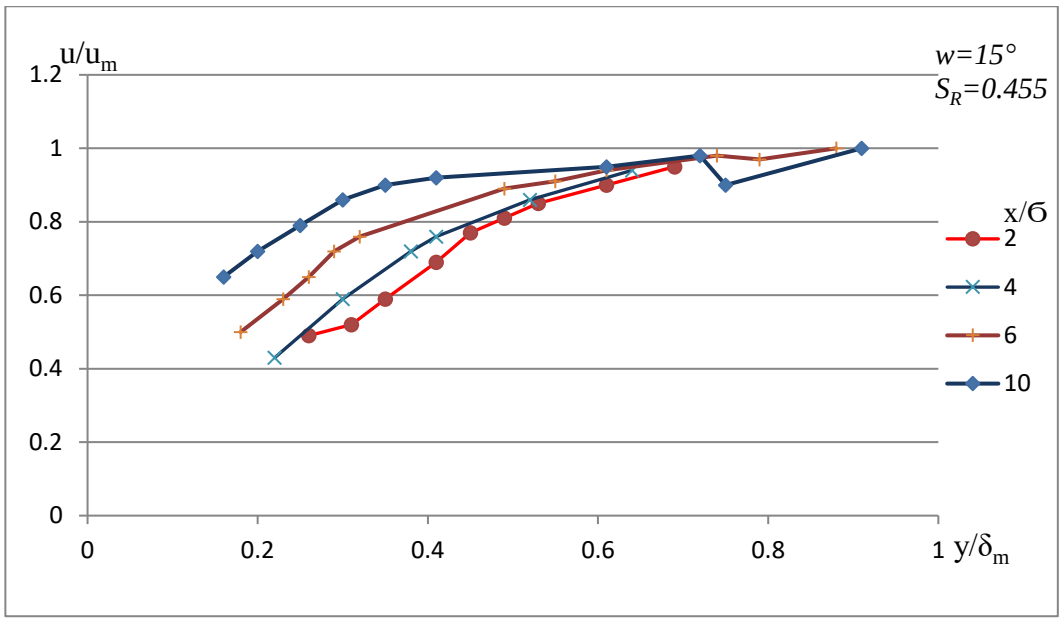

Fig. 20. Velocity profiles in the wall boundary layer of a conical diverging stream

In a converging jet, the maximum of the velocity profile is much faster moving away from the cone wall than in similar sections of a diverging jet.

The change in the maximum velocity u_m and the nominal thickness of the jet $\delta_{0.5}$ along the length of the conical jet for different values of the transverse curvature parameter of the streamlined surface S_R and the cone opening angle w *are* shown in Figures 22 - 24. As can be seen, the thickness of the jet in a diverging conical and radial jet increases linearly with distance from the nozzle, and the value of the coefficient of proportionality $\boldsymbol{c}$ in the formula $\delta_{0.5} = cx$ [46] does not depend on the opening angle of the cone, whereas according to the calculated dependence for xsinw >> R in a diverging jet, the jet thickness should be in two and times less than in a flat semi-limited jet at the same distance from the nozzle. Similarly, a decrease in the thickness of the radial free jet was obtained in the calculations of A.S. Ginevsky [47]. In a converging jet along the cone and the disk, the thickness of the jet grows nonlinearly with distance from the nozzle, qualitatively in accordance with the dependence. The maximum speed of a jet in a diverging jet decreases faster than in a flat semi-limited jet. However, this dependence cannot be described with satisfactory accuracy by both formula (71) and (73).

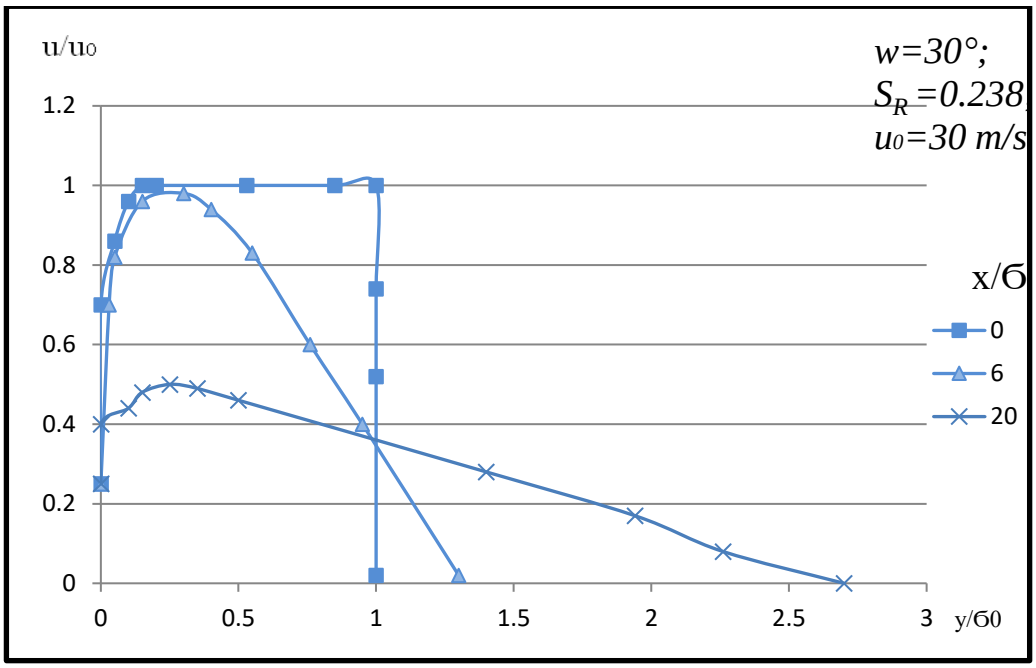

Fig. 21. Velocity profiles in a diverging conical stream

Therefore, based on these calculated dependences, taking into account the experimental data for plane, cylindrical, conical, and radial jets, the following semi-empirical formula was chosen (81):

$$\frac{u_m}{u_0} = \frac{0.61\,\mathrm{Re}_0^{0.06}(1+0.5S_R\cos\omega)^{0.55}}{\left\{\frac{\delta_{0.5}}{\sigma}\left[1 \pm S_R\frac{x}{\sigma}\sin\omega + 0.152\,\mathrm{Re}_0^{0.11}\cdot S_R\left(\frac{\delta_{0.5}}{\sigma}\right)^n\cdot\cos\omega\right]\right\}^{0.55}}, \tag{81}$$

where $n = \frac{1+0.082S_R}{1+0.10S_R}$, $n = \frac{u_0\cdot\sigma}{\nu}$.

The thickness of a semi-limited jet propagating along flat, cylindrical and conical (diverging) surfaces with an accuracy of $\mp$10% is described by the dependence (82):

$$\frac{\delta_{0,5}}{\sigma} = 0{,}070\left(\frac{x}{\sigma}+\frac{x_n}{\sigma}\right). \tag{82}$$

In converging conical and radial wall jets, the thickness of the jets in the main section is determined by the dependence (83):

$$\frac{\delta_{0,5}}{\sigma} = 0{,}070\left(\frac{x}{\sigma}+\frac{x_n}{\sigma}\right)\frac{1-0.474S_R\frac{x}{\sigma}\cdot\sin\omega+0.146S_R\frac{x}{\sigma}\cdot\cos\omega}{1-S_R\frac{x}{\sigma}\cdot\sin\omega+0.146S_R\frac{x}{\sigma}\cdot\cos\omega}, \tag{83}$$

where x_n is the pole distance of the jet .

A comparison of the calculated dependences (82) - (83) with the experimental results of this work and other authors is shown in Fig. 3.7 and 3.8. In fig. 3.9, experimental data on changes in the maximum velocity in diverging jets and jets propagating along the surfaces of the plate and cylinder are constructed. The graphs for comparison show the results of the calculated dependence (78) (solid lines). An analysis of these graphs (23-24) shows that the change in the

maximum velocity in semi-limited jets is described by both formula (79) and formula (81), with an error not exceeding ∓10%.

In the calculation formulas for the maximum speed of a diverging jet along the cone, the parameters of conicity and transverse curvature are in the form of the product $S_R \cdot \sin\omega$. Therefore, if the product is the same for conical and radial jets, then the maximum speed and width of the jets should change almost the same.

Indeed, as can be seen from the data presented in Figs. 22 and 23, the parameter $S_R \cdot \sin\omega$ is decisive. If this parameter is greater for the jet along the cone than for the radial diverging jet, then the maximum velocity in the jet along the cone decreases faster than in the radial diverging jet.

Figure 24 compares the calculations using formulas (73), (74) and (79) and the Sharma formula with the experimental data of the radial and conical diverging jets. As can be seen, formulas (73) give overestimated values of the velocity. E then due to the fact that (74) of the jet width decreases with increasing angle of taper and charm formula is derived without considering the frictional forces streamlined surface.

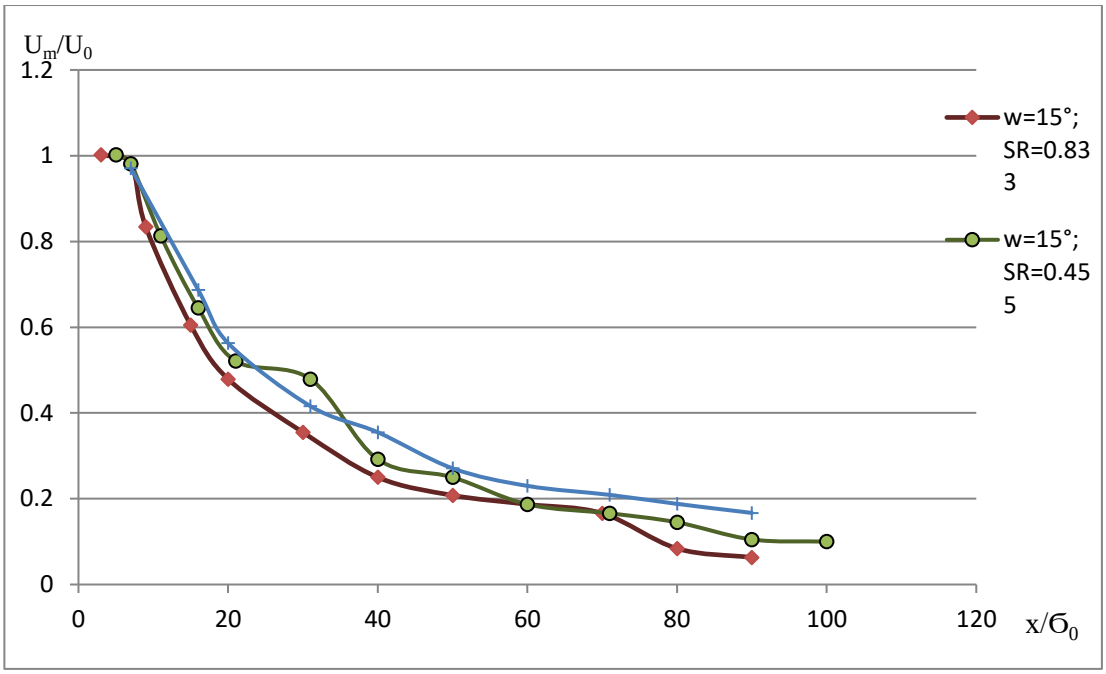

Fig. 22. Change in maximum speed at various S_R

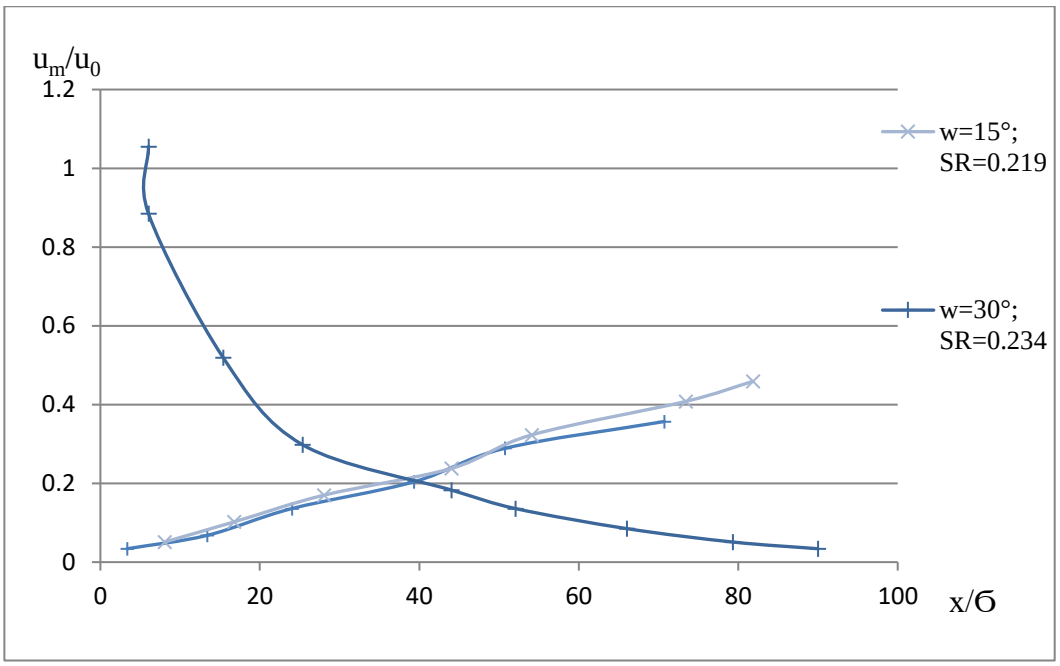

Fig. 23. Change in maximum speed and jet boundary

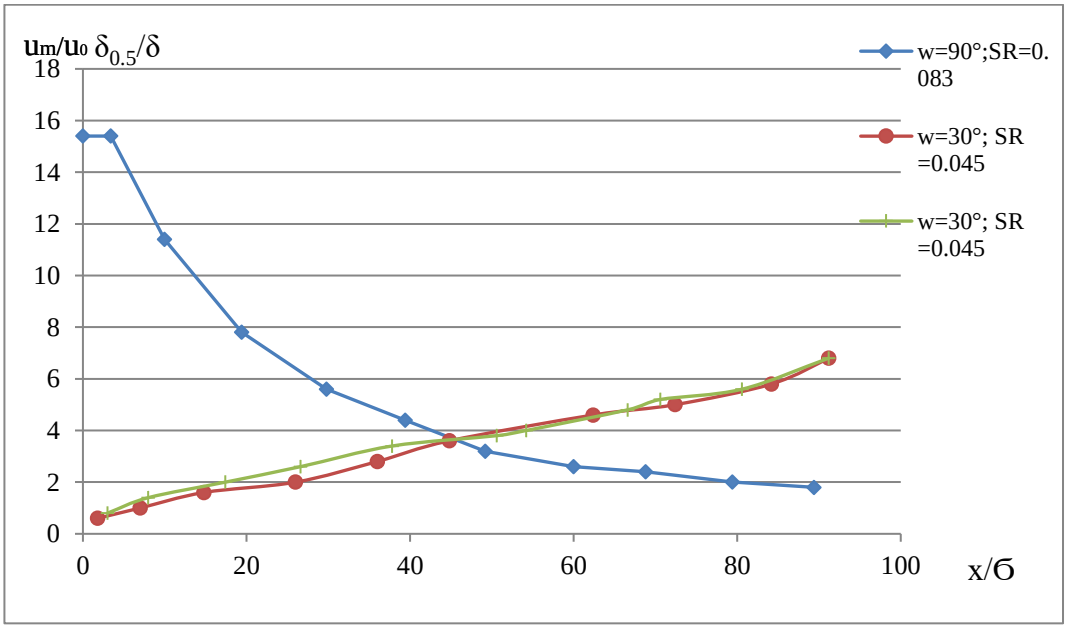

Fig. 24. Comparison of the results of calculation formulas with experimental data

Formula (78) accurately describes the experimental dependences.

It is known that the geometry and dynamics of the initial section of the jet significantly influence the formation of the boundary layer in the main section. In order to elucidate such an effect, the initial section of the diverging jet was studied in detail. A more detailed measurement of the average velocity profiles in the initial section of the jet propagating from the top of the cone towards its base showed that the conditional thickness of the boundary layer along the length of the initial section decreases markedly. This phenomenon can be explained as follows. Just as in a flat wall jet in the initial section of the stream, its thickness is much smaller than the length of the initial section and it can be assumed that the pressure in the initial section is constant and equal to atmospheric pressure. Then there is no reason to change the speed along its length. Therefore, within the core of constant speeds $P = const$ and $u=u_0=const$. The change

in the thickness of the core of constant velocities within the initial section can be found on the basis of the constancy of the jet momentum, neglecting, to a first approximation, the effect of friction on the streamlined surface.

The patterns of jet propagation in the mixing layer in the initial section of the jet along the cone are assumed to be the same as in a plane jet in accordance with G.N. Abramovich [1], i.e. $\delta_n = 0.27x$. Then, for a quantitative description of the parameters of the initial section on the basis of a semi-empirical calculation, we obtain the following formulas:

for the boundary of constant speeds there is a formula (84):

$$\frac{y_0}{\sigma} = \frac{\sqrt{(1 \pm S_R \frac{x}{\sigma} \sin\omega)^2 + S_R \cos\omega(2 + S_R \cos\omega)} - (1 \pm S_R \frac{x}{\sigma} \cdot \sin\omega)}{S_R \cdot \cos\omega} - 0.112\frac{x}{\sigma}. \quad (84)$$

for the conditional jet boundary in the initial section (85):

$$\frac{\delta_{0,5H}}{\sigma} = \frac{\sqrt{(1 \pm S_R \frac{x}{\sigma} \sin\omega)^2 + S_R \cos\omega(2 + S_R \cos\omega)} - (1 \pm S_R \frac{x}{\sigma} \cdot \sin\omega)}{S_R \cdot \cos\omega} + 0.027\frac{x}{\sigma}, \quad (85)$$

for full jet boundary (86):

$$\frac{\delta_0}{\sigma} = \frac{\sqrt{(1 \pm S_R \frac{x}{\sigma} \sin\omega)^2 + S_R \cos\omega(2 + S_R \cos\omega)} - (1 \pm S_R \frac{x}{\sigma} \cdot \sin\omega)}{S_R \cdot \cos\omega} + 0.158\frac{x}{\sigma}. \quad (86)$$

At the end of the kernel of constant speeds $\frac{y}{6} = 0$, from (84) we obtain the length of the kernel of constant speeds (87):

$$\frac{x_H}{\sigma} = 8.93\frac{\pm\sqrt{1 + (2 + S_R \cos\omega)(\cos\omega \pm 17.86\sin\omega)S_R} - 1}{(\cos\omega \pm 17.86\sin\omega)S_R}. \quad (87)$$

Assuming x '= x + x_n for the main section of the jet, where x is the distance from the nozzle exit, x_n is the pole distance, which is found from the condition of coincidence, the thickness of the jet at the end of the initial section according to (85) with the jet thickness of the main section according to the formula (84) for x = $x_н$, we obtain (88):

$$\frac{x_n}{\sigma} = 14.3\frac{\delta_{0.5H}}{\sigma} - \frac{x_H}{\sigma}. \quad (88)$$

In the above formulas, the calculations were performed taking into account the pole distance found from (88).

$$\frac{u}{u_0}\frac{1}{S_R^{1/3}} = f(\frac{r'}{R}) \quad (89)$$

and

$$\frac{2\Delta P_{cm}}{\rho u_0^2}\frac{1}{S_R^{1/3}\sin^{2.5}\omega} = f(\frac{x}{R}\sin\omega) \quad (90)$$

3.3 The development of turbulence in the wall jet

Experiments to study the turbulent structure were carried out on the setup shown in Figure 4, and the value of the velocity ripple was measured on the setup on which the averaged velocity profiles were measured.

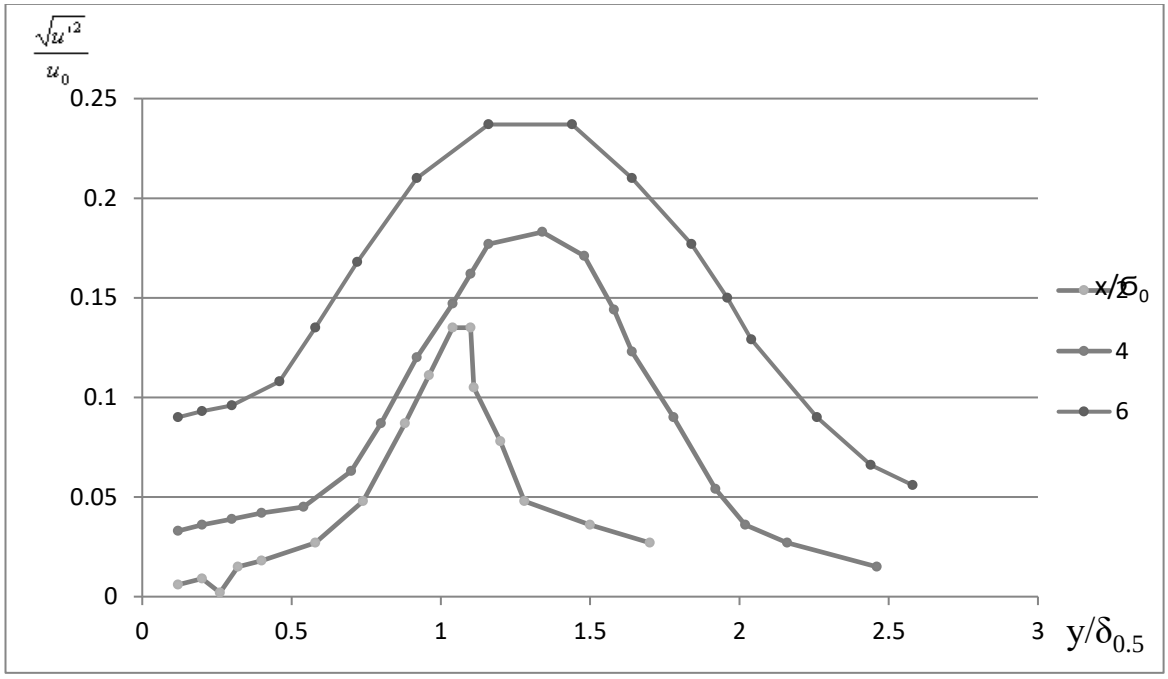

Fig. 25. Profiles of ripple of longitudinal velocity in a diverging conical stream

The longitudinal velocity pulsation profiles, referred to the initial velocity, as a diverging conical jet at w = 30 ° are shown in Figure 25. As can be seen from the figures, the maximum value of the velocity pulsations is achieved in the diverging stream at $\frac{y}{\delta_{0.5}}$ =1.0-1.9 and then remains without changes.

Distribution of longitudinal velocity pulsations, related to the maximum velocity in the section, along the line of maximum velocity of the wall jets. When the jet is distributed along the cone towards its base, the level of jet turbulence along the line of maximum speed is much higher than in a plane semi-limited jet and approaches its value on the axis of a free round jet, while in a converging conical and radial jets the turbulence level becomes much lower than in a flat semi-limited jet. The dimensionless velocity pulsation profiles, referred to the local velocity value in a radial semi-limited jet, show that the level of turbulence in a diverging radial jet can be even greater; than in a round free stream not only on the axis of the stream, but also over the entire width of the stream. Apparently, an increase in the turbulence in the divergent jets neutralized decrease the width of the jet by increasing the flow cross-section, whereby the width of intensity of the growth divergent jets is the same as that of flat planes. An analysis of our own experimental data and works of other authors made it possible to obtain an empirical dependence for describing changes in the level of turbulence along the line of the maximum velocity of semi-limited jets and a round free stream in the form (91):

$$\varepsilon_u = \frac{1}{2}\left[0.03 + 0.25(1 \pm 0.667\sqrt{\frac{\sin\omega}{1 \mp 0.937\sin^{0.2}\omega}}) \cdot (1 - e^{-0.11\left(\frac{x}{\sigma}\right)^{0.8}})\right] \cdot \left[1 + \cos^2\omega \cdot th(0.0142 \cdot S_R \frac{x}{\sigma})\right]. \quad (91)$$

Here, the upper signs correspond to a diverging stream.

The dependence of the degree of periodicity F(f) on the vortex formation frequency at w = 15° and S_R = 0.71. As can be seen, directed acoustic exposure with a frequency corresponding to the frequency of formation of large-scale vortices in the outer boundary layer at the end of the initial section significantly enhances the intensities of coherent structures and high-frequency exposure, on the contrary, reduces the intensity of the vortices. This effect is clearly visible in photographs of the vortex flow pattern shown in Figure 26. It can be seen that at low frequencies of sound exposure, large vortices are first formed, reaching maximum intensity at a resonant frequency that coincides with the frequency of natural vortex formation. With a further increase in the frequency of acoustic exposure, the vortex intensity decreases and its effect on the development of the jet weakens. The influence of acoustic exposure is stronger for a converging jet than for a diverging jet at the same frequency and intensity of exposure.

To determine the flow region with the most pronounced periodicity, we measured the distribution of F(f) along the line of the maximum velocity and the cross section of the jet.

Stepped the dependence of the Strouhal number S (Re) , obtained for the onset of the field perturbation at the outer edge of the initial portion of the jet, due to the presence in the spectra of several maxima. The characteristic frequency having the largest amplitude was determined by both corresponding frequencies and two values connected by a vertical line were plotted.

The regularity of the change in S_1 can be described by the formula $S_1=k\sqrt{Re}$, where k is 0.164, a constant depending on the geometry of the nozzle and the initial flow conditions. According to the data of [11], for a plane semi-bounded jet, k = 0.0122, and in [34] for a free jet this coefficient was equal to k=0.0195.

The experimental values of the Strouhal number $S_m = \frac{f_m b}{u_0}$ for the characteristic frequency f_m, identified by the spectrum in the region most clearly expressed a large-scale frequency on line maximum speeds are stacked in the interval 0,18-0, 25. From the observation and photographing shadow pattern currents under pulsed irradiation was found that when Re = $(7 \div 9)\ 10^3$ large area of large-scale vortices formed by the periodicity of the two pairwise fusions small eddies arising in the nozzle from the edge of the separated boundary layer outer free primary jet. After the first merger, doublet structures are formed. At Site $3 \cdot 10^3 < Re < 5 \cdot 10^3$ forming the field current to a large-scale periodicity is realized in basically the pairwise merge. At Re $\cdot 5\ 10^3$, large eddies are formed at the end of the initial section by two pairwise mergers of smaller eddies that have developed upstream.

In the region of $1.5 \cdot 10^3 < Re < 3 \cdot 10^3$, the development of long-wave vortex disturbances in the outer mixing layer of the initial section is characteristic. During its development, interacting in pairs and merging into larger eddies, towards the end of the initial section of the jet generate a characteristic frequency of velocity pulsation with the Strouhal number S_m = $0.22 \div 0.27$.

Thus, coherent structures that have developed towards the end of the initial section of the jet represent a complex system of merging vortices. The number of vortices in this system grows with increasing Reynolds number.

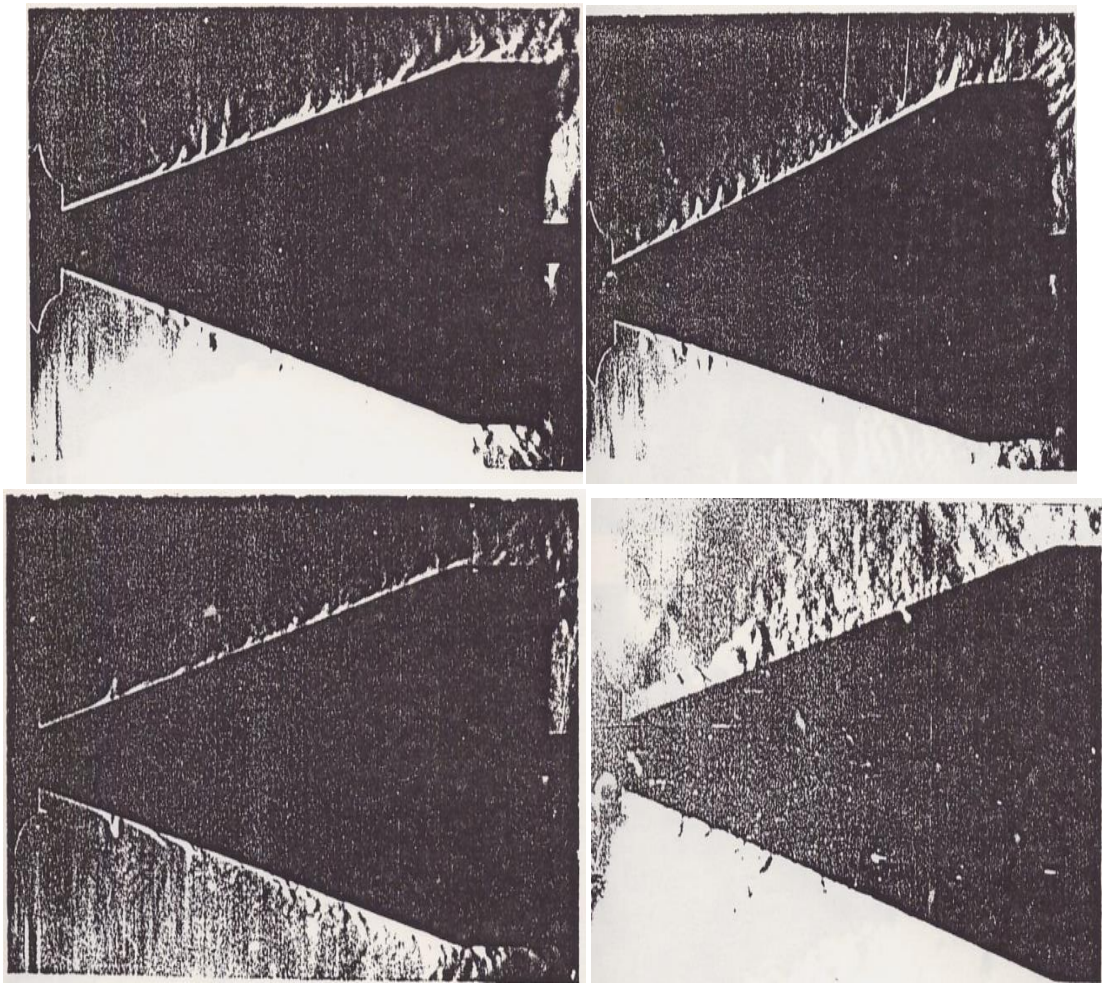

Fig. 26. Tepler images of coherent structures in a diverging stream

Conclusions

1 The effect of the geometry of a streamlined surface on the aerodynamics of a wall radial jet and a jet propagating over the surface of a cone (diverging) in a range of parameters is studied in detail .- $\frac{\pi}{2} \leq w \leq +\frac{\pi}{2}$,$0 \leq S_R \leq 1.0$, $10^3 < Re_0 < 10^5$

2 It has been established that dimensionless velocity profiles in the sections of the main section in coordinates = f (y / $\delta_{0.5}$) for all the considered modes are almost self-similar. However, the absolute transverse velocity gradients in the near-wall region increase with increasing parameters S_R and w for diverging jets. At the same time, the dimensionless velocity profiles in the wall region in the coordinates $\frac{u}{u_m}$= f (y /δ_m) in the diverging conical jet are less filled.

3 It is shown that the change in the total thickness of the jet along its length occurs identically for a flat, cylindrical and conical diverging jet and obeys the dependence = 0.070x. Based on the analysis of experimental data and approximate calculations, generalizing dependences for changing the maximum speed and thickness of a wall diverging conical jet are obtained, taking into account the influence of the transverse curvature parameter S_R, the opening angle w and the initial Reynolds number Re_0, which also describe a wall jet along the cylinder at $w = 0$ and flat wall at $S_R = 0$.

4 Experimental studies and experiments and approximate calculations showed that the length of the core of constant velocities in a diverging stream decreases. In accordance with this, the extent of the region of formation and development of coherent vortex structures in the initial section of the jet also changes.

5 In detail, the vortex structure and the development of turbulence in a diverging conical jet are investigated. It has been established that discrete vortex structures are also formed in the initial section of the conical jet, the formation frequency of large vortices is measured, and the possibilities of controlling their intensity with the help of acoustic influence are studied. The change in the level of turbulence over the sections is studied and a generalized formula for the level of turbulence along the line of the maximum velocity is obtained, taking into account the influence of the parameter S_R, the angle w, and the direction of flow of the wall jet. The obtained dependences within the experimental accuracy of 10% describe all the experimental data in the range of parameters: $0 \leq S_R \leq 100$, $-\frac{\pi}{2} \leq w \leq +\frac{\pi}{2}$, $10^3 < Re_0 < 10^5$

List of references

1 ABRAMOVICH, Gabriel. *Theory of turbulent jets.* Science, 1984. ISBN-13: 978-0262010085.

2 KONDRASHENKO S. I., PRIBYTKOV I. A. Structure of the flow and aerodynamics of a jet interacting with normality with a restricting surface. "*MISiS" National Research Technological University*. Moscow: 2018.

3 ANDERSON, John D., Fundamentals of Aerodynamics. 5th edition. McGraw-Hill Series in Aeronautical and Aerospace Engineering, 2011. ISBN 978-0-07-339810-5.

4 GORDA, R. Influence of transverse curvature on flows in a laminar wall jet. *Theoretical Foundations and Engineering Calculations.* 1975, 1, p. 171-173.

5 ISSATAYEV, Sovet. *Propagation of the laminar floor of a restricted jet flowing from an annular source of finite diameter along cylindrical, conical, and spherical surfaces.* Alma-Ata: Applied Thermophysics, 1965.

6 KASHKAROV, Vasily, L.Yu., ARTYUKH. *Propagation of the laminar stream of a compressible gas along the surface of a cone*. Alma-Ata: Investigation of transport processes, 1960.

7 SCHAUER, James Jay, MYERS, G.E., JUSTIS R.H. *Development of flow and coefficient of friction in a semi-infinite flat turbulator coagulant minutes jet*. Technical mechanics, 1963.

8 MAKAROV V. N., GORBUNOV S. A., KOMILOVA T. A. Method of calculating angle of disclosure of the interdoor channel of the working wheel of shaft fan. 2013.

9 ISSATAYEV, Sovet. *Propagation of a turbulent semi-limited jet along a flat plate.* Alma-Ata: Physics. 1968, 3, p.102-108.

10 LAUNDER, Brian and RODI, Wolfgang. The Turbulent Wall Jet. *Progress in Aerospace Sciences* [online]. 1981,v.19, p.81-128. Retrieved from: doi: 10.1016/0376-0421(79)90002-2

11 KUNAKBAEV, Tuleugali. *Hydrodynamics and heat exchange semibounded flat jet with a cocurrent flow with a longitudinal pressure gradient pressure*. Alma – ata: 1984, p. 20.

12 BEKTURGANOV Ersultan., DZHAUGASHTIN, Kazbek, SAKIPOVA, Zuryadda. The problem of a laminar semi-limited stream of incompressible fluid along a moving plate. *Bulletin of the Academy of Sciences of the Kazakh SSR*. 1974,no. 9.

13 ISSATAYEV, Sovet, ABDRAKHMANOVA, Roza. On the development of a wall boundary layer in a turbulent plane semi-limited jet. *Applied and Theoretical Physics.* 1974, vol. 6, p.262-269.

14 CHAOQUN Liu, PING Lu. New Theories on Boundary Layer Transition and Turbulence Formation. *Modelling and simulation in engineering* [online]. 2012, p. 22. [accessed 25 March]. Retrieved from: doi.org/10.1155/2012/619419

15 ISSATAYEV, Sovet, SOLTANBAEV, Sh. On the effect of transverse curvature on the laws of a jet propagating along a cylindrical surface. *Hydrodynamics and diffusion*. Alma-Ata: 1982, p.63-71.

16 SAKIPOV, Z.B., RYABININ, V.P., KOZHAKHMETOV, D.B. Investigation of the pulsation characteristics of turbulent jets propagating along a flat smooth and rough surface. *Problems of heat power engineering and applied thermophysics*. Alma-Ata: 1974, no. 10, p. 87-95.

17 SADOVNIKOV, D.V., SMOLSKY, B.M., SHCHITNIKOV, V.K. Development of the flow and pulsation characteristics of a plane semi-bounded jet. *Aerothermooptics and beam guides*. 1970, p.229-244.
18 KOKUNINA L.Kh. Fundamentals of aerodynamics. 2015. ISBN978-5-91872-097-4
19 MONIN, Andrey and Akiva YAGLOM. Statistical hydromechanics. Moscow: Science, 1965.
20 VOLKOV K.N. The interaction of a circular turbulent jet with a flat barrier. *Applied Mechanics and Technical Physics*. 2007, vol.48, No. 1, p. 55-67.
21 BASHKIN V.A. EGOROV I.V. Numerical study of external and internal aerodynamics problems. *Fizmatlit*. Moscow: 2013. ISBN 978-5-9221-1524-7
22 *Hydrodynamic instabilities and the transition to turbulence*. Ed.By Swinney H. and Gollub J. Moscow: Mir, 1984.
23 GOLDSHTICK, Michael A. Dynamic equilibrium and flow structures of turbulence. *Structural turbulence.* Novosibirsk: Collection of scientific interpretations, 1982.
24 E.R van DRIEST, BLUMER, C.B. Boundary layer transition-freestream turbulence and pressure gradient effects. *AIAA Journal* [online]. 1963,no. 6, p.25-29.[accessed 17 May 2012]. Retrieved from: doi.org/10.2514/3.1784
25 STARR, J.B., SPARROW, Ephraim M. Experiments on a turbulent cylindrical wall jet. *Journal of Fluid Mechanics.* 1967, vol.29, no.3, p.495-512. Retrieved from:doi.org/10.1017/S0022112067000990
26 ISSATAYEV, Sovet. Experimental Investigation about a Laminar - Turbulent Transition in Free and semi Limited Jet Flow Is Laminar.*Turbulent Transition, S pringer-verlag*. 1984 Berlin - Hede berg – the New York – Tokio. p. 11-418.
27 LAU J.C and FISHER M. J. The vortex - street Structure of Turbulent jets. *Journal of Fluid Mechanics*[online].1975, vol.67, p.299-337. [accessed 29 March 2006]. Retrieved from: doi.org/10.1017/S0022112075000328
28 ISSATAYEV, Sovet and Sergey B., TARASOV. On the characteristic frequencies in the spectra of the velocity pulsations of the initial section of axisymmetric jets. 4th edition. Alma-Ata: In Collection of Applied and Theoretical Physics, 1973.
29 DAVIES, Paul and Andrew, YULE. Coherent Structures in Turbulence. *Journal of Fluid Mechanics* [online]. 1975, vol.69, p. 513-537. [accessed 29 March 2006]. Retrieved from:doi.org/10.1017/S0022112075001541
30 SAKIPOV, Z.B., RYABININ, V.P. The investigation of the influence of low-frequency oscillations on the development of a wall jet and a diffusion gas plume. Alma-Ata: 1976, vol. 11, p.99-111 .
31 ERSHIN, Shahbaz A. and LUCHINSKY, S.F. Investigation of the turbulent structure of a flat layer of mixing satellite streams with initial velocity profile irregularity. *In the book: Turbulent jet flows.* Academy of Sciences of the ESSR, Tallinn: 1979, part 1, p.103-113.
32 VLASOV, Evgeny V. and Alexander V., GINEVSKY. Acoustic effects on the aerodynamic characteristics of a jet. *USSR Academy of Sciences*, MZHG. 1967, no.4.
33 ISSATAYEV, Sovet and Sergey B., TARASOV. On the action of an acoustic field directed along the axis of a jet on a jet. *USSR Academy of Sciences, MX*. 1971, no.2, p.164-167.
34 ISSATAYEV, Sovet and Sergey B., TARASOV. Investigation of the vortex structure of the flow in the transition region of free jets with superimposed small influences. *Collection Thermophysics and Radiation Physics.* Alma-Ata: 1979, vol.2.

35 ISSATAYEV, Sovet, MUKHAMEDIN S.M. Visual studies of the effect of sound on a homogeneous torch. *In the book: Applied and Theoretical Physics*. Alma-Ata: 1976, vol.7, p.194-197.
36 KRASILNIKOVA, Tatyana K., Oleg A., LAVRISHCHEV. Correlation characteristics of turbulence in a fan near- wall jet. *NIINTI*. Alma-Ata: 1987, No. 1665-Ka87, p.7.
37 LOGACHEV I.N., LOGACHEV K.I. *Aerodynamic principles of aspiration. Monograph.* St. Petersburg: Khimizdat, 2005. p.659.
38 Gas dynamics. Favorites. T. 1. Under the general ed. A.N. Kraiko. 2nd edition - M.: Fizmatlit, 2005. - p.720.
39 IDELCHIK, I.E. Aerodynamics of industrial apparatus. *Energy*. Moscow: 1964.
40 POVH, Ivan L. Aerodynamic experiment in mechanical engineering. *Engineering*. Leningrad: 1977.
41 INSHAKOV S.I. Visualization of the structure of gas flows by shadow and interference methods. *Bulletin of the Samara State Aerospace University*. 2007, no.2, p.108-112.
42 JOUNG-Ho, LEE Hyung, JIN Sung. Obtaining accurate mean velocity measurements in high Reynolds number turbulent boundary layers using Pitot tubes. *Journal of Fluid Mechanics* [online]. 2013, vol.715, p.642–670. [accessed 27 October 2012]. Retrieved from:doi:10.1017/jfm.2012.538
43 SARPKAYA Turgut. Effect of the Adverse Pressure Gradient on Vortex Breakdown. *AIAA journal*. Vol.12, issue 5. [accessed 17 May 2012]. Retrieved from: doi.org/10.2514/3.49305
44 DOLINSKY, E.F. Processing of measurement results. *Publishing house of standards*. Moscow: 1973, .p.192
45 ISSATAYEV, Sovet I., BERDIBAEV, M.S., KUNAKBAEV, TULEUGALI K. An experimental study of the influence of a longitudinal pressure gradient, confusion, and the shape of a streamlined surface on the aerodynamics and heat transfer of semi-limited jets. *In book: Wall jets flows*. Novosibirsk: 1984, p.24-28.
46 Sharma R.N. An experimental study of conical wall currents. 1981, no.1, vol.19.
47 BERDIBAEV, M.S. Investigation of the aerodynamics of a semi-boundary jet propagating along a conical surface. *Abstract of the Scientific Conference on the Report of the Academy of Sciences of the Republican Inter-University Mathematics and Mechanics.* Alma-Ata: 1984, part 111, p.131.

Application 1. The distribution of velocity in the cross section of a conical and radial wall jets

w=	15°;	б=5.0	mm;	S_R=0.455;			u_0=30 m/s			
	y, mm	Δh, mm	y, mm	Δh, mm	y, mm	Δh, mm	y, mm	Δh, mm	y, mm	Δh, mm
x/ б	0;	k=0,6	2		4		6		10	
	1		2		3		4		5	
	0.13	76	0.13	55	0.13	45	0.13	58	0.13	68
	0.16	84	0.16	65	0.16	60	0.16	78	0.16	72
	0.18	110	0.18	82	0.18	80	0.18	98	0.18	85
	0.20	137	0.20	110	0.20	100	0.20	115	0.20	102
	0.22	161	0.22	135	0.22	120	0.22	128	0.24	120
	0.24	178	0.24	154	0.24	133	0.24	140	0.28	130
	0.26	190	0.26	172	0.26	145	0.26	150	0.32	138
	0.28	200	0.28	184	0.28	155	0.30	163	0.36	143
	0.30	207	0.30	195	0.30	173	0.34	178	0.40	147
	0.32	212	0.32	207	0.32	190	0.38	191	0.44	150
	0.34	218	0.34	215	0.34	195	0.42	198	0.48	153
	0.36	222	0.36	219	0.38	210	0.46	204	0.56	155
	0.38	224	0.38	221	0.42	216	0.50	210	0.60	156
	0.40	225	0.42	223	0.46	220	0.54	213	0.64	157
	0.42	226	0.46	225	0.50	222	0.62	215	0.80	158
	0.44	227	0.50	227	0.62	227	0.74	219	1.10	155
	0.48	228	0.54	228	1.78	224	0.76	220	1.20	153
	4.52	228	3.78	228	1.86	223	1.20	218	1.30	150
	4.62	225	3.80	227	2.00	221	1.30	215	1.60	145
	4.72	214	3.86	225	2.20	218	1.40	212	1.80	140
	4.76	205	3.92	220	2.30	215	1.50	207	2.20	128
	4.78	199	3.98	214	2.50	208	1.70	199	2.60	113
	4.80	190	4.04	202	2.70	199	2.00	187	3.00	100
	4.84	167	4.10	193	2.90	188	2.20	179	3.40	85
	4.88	140	4.16	182	3.10	175	2.40	168	3.80	73
	4.90	118	4.22	170	3.30	160	2.60	155	4.20	63
	4.92	97	4.28	153	3.50	144	2.80	142	4.40	56
	4.94	78	4.34	135	3.70	123	3.00	130	4.50	53
	4.96	62	4.40	120	3.90	108	3.20	120	4.60	51
	5.00	45	4.46	100	4.10	88	3.40	108	4.80	49
	5.04	18	4.52	80	4.30	73	3.60	98	4.90	47
	5.08	0	4.54	74	4.50	56	4.00	78	5.00	44
			4.56	66	4.60	48	4.30	66	5.10	43
			4.58	60	4.70	42	4.40	57	5.30	38
			4.60	54	4.90	30	4.50	54	5.70	30
			4.62	50	5.10	22	4.60	50	6.90	15
			4.64	42	5.50	8	4.80	43	8.00	3

			4.66	37	5.70	2	5.00	36		
			4.72	28			5.40	26		
			4.80	18			6.20	10		
			5.20	5			7.20	2		
			5.50	1						

w=30°;	б=5.0 mm;				S_R=0.455;		u_0=30 m/s			
	y, mm	Δh, mm	y, mm	Δh, mm	y, mm	Δh, mm	y, mm	Δh, mm	y, mm	Δh, mm
x/ б	0;	k=0,4	2		4		6		10;	k=0.2
	1		2		3		4		5	
	0.134	155	0.134	133	0.134	115	0.134	115	0.134	108
	0.160	166	0.160	141	0.160	121	0.160	111	0.160	212
	0.180	177	0.180	153	0.180	135	0.180	123	0.180	225
	0.200	183	0.200	165	0.200	147	0.200	133	0.200	235
	0.220	194	0.220	176	0.240	168	0.220	142	0.220	243
	0.240	202	0.240	183	0.260	177	0.240	150	0.240	252
	0.260	206	0.260	190	0.280	185	0.260	157	0.260	258
	0.300	210	0.280	197	0.300	191	0.280	168	0.300	262
	0.340	213	0.300	202	0.320	195	0.300	172	0.340	270
	0.380	214	0.340	208	0.340	200	0.340	179	0.380	275
	0.420	215	0.400	213	0,360	207	0.380	191	0.420	283
	0.460	216	0.440	214	0.380	213	0.420	197	0.460	282
	0.500	216	0.500	215	0.400	214	0.460	203	0.500	284
	0,600	216	0.560	216	0.400	215	0.500	205	0,600	287
	0,800	217	0,620	217	0.480	215	0,540	210	0,700	288
	1,00	218	0,700	217	0.600	217	0,580	211	0,800	290
	1,400	218	0,800	217	0,800	218	0,700	212	0,900	290
	2,00	219	0,900	217	1.000	218	0,800	213	1,000	288
	4.400	218	1,00	218	1,200	218	0,900	210	1,100	285
	4.440	217	1,200	218	1,600	218	1,100	208	1,200	283
	4.500	216	1,400	219	2,000	217	1,200	205	1,300	280
	4.600	207	2,000	219	2,200	214	1,300	203	1,400	275
	4.700	180	3,000	219	2,400	205	1,400	201	1,500	207
	4.740	165	3,600	219	2,600	198	1,600	195	1,700	255
	4.780	145	3,800	205	2,800	190	1,800	184	1,800	250
	4,820	113	3,900	180	3,000	172	2,000	176	2,000	240
	4,840	97	3,960	172	3,200	158	2,200	168	2,200	225
	4,860	80	4,000	161	3,400	135	2,400	158	2,400	213
	4,880	55	4,060	142	3,600	120	2,600	145	2,600	203
	4,900	37	4,120	123	3,800	100	2,800	135	2,800	193
	4,920	15	4,180	100	3,900	85	3,000	120	3,000	173

	4,940	8	4,220	85	4,000	78	3,200	165	3,200	165
	4,960	3	4,240	80	4,100	70	3,400	98	3,600	140
	5,000	0	4,260	72	4,200	60	3,600	85	4,000	115
			4,280	65	4,300	52	3,800	75	4,200	105
			4,300	60	4,400	40	4,000	65	4,400	98
			4,320	54	4,500	32	4,100	58	4,760	90
			4,340	48	4,600	28	4,200	53	4,800	80
			4,360	40	4,800	16	4,300	48	5,000	70
			4,380	35	5,000	5	4,400	44	5,900	60
			4,420	27	5,200	0	4,600	35	5,400	58
			4,480	15			4,800	28	5,600	52
			5,000	0			5,000	24	6,000	37
							5,200	20	6,400	30
							5,600	10	7,000	15
							6,000	5	7,600	8
							6,400	2	8,200	3